ELSEVIER

Marine Geology 215 (2005) 59–92

MARINE GEOLOGY
INTERNATIONAL JOURNAL OF MARINE GEOLOGY, GEOCHEMISTRY AND GEOPHYSICS

www.elsevier.com/locate/margeo

Mechanical models of the 1975 Kalapana, Hawaii earthquake and tsunami

Simon J. Day[a,*], Philip Watts[b], Stephan T. Grilli[c], James T. Kirby[d]

[a]*Benfield Hazard Research Centre, Department of Earth Sciences, University College London, Gower Street, London WCIE 6BT, UK*
[b]*Applied Fluids Engineering, 5710 E. 7th Street, Long Beach, CA 90803, USA*
[c]*Ocean Engineering, University of Rhode Island, Narragansett, RI 02882, USA*
[d]*Center for Applied Coastal Research, University of Delaware, Newark, DE 19761, USA*

Accepted 8 November 2004

Abstract

Our objective is to produce a mechanically realistic model for the 1975 Kalapana event that explains the overall deformation and geological evolution of the south flank of Kilauea, and reproduces most known earthquake and tsunami observations. To do this, we present a new structural interpretation of geological data from Kilauea, along with modeling of the tsunami using recent seismic analyses. In so doing, we hypothesize an offshore north-facing normal fault that we call the Kalapana fault, because of its limited onshore expression near Kalapana. We argue that several different interpretations of seismic data are simultaneously true, each coinciding with a specific geological structure. We perform a direct numerical simulation of the 1975 Kalapana tsunami, and we report results for the near field and the far field simultaneously. Our interpretation of geological structures provides sufficient constraints to derive three tsunami sources: the Kalapana fault, a slump, and a thrust fault. These three tsunami sources are mechanically coupled according to our model of Kilauea evolution, although their contributions to tsunami generation remain relatively distinct. Slump displacement predicts a small shear stress beneath Kilauea volcano. We find that our geological interpretation and tsunami sources are sufficiently robust to reproduce almost all tsunami observations. Repeated earthquakes like the 1975 Kalapana event will produce extension and subsidence in the upper flank of Kilauea, as well as compression and uplift of the toe region, accompanied by limited slump movement. These deformations appear to stabilize Kilauea and make catastrophic failure of the volcano flank less likely at this time.

Keywords: Kalapana; Hilo; Kahului; Honolulu; Hilina; Hawaii; earthquake; slump; tsunami; volcano; Kilauea; extension; subsidence; thrust; landslide; shear stress; observation; prediction; generation; propagation; runup

* Corresponding author. Now at Institute of Geophysics and Planetary Physics, UC Santa Cruz, Santa Cruz, CA 95064, United States. Tel.: +44 171 504 2212; fax: +44 171 380 7193.
E-mail address: sday@es.ucsc.edu (S.J. Day).

0025-3227/$ - see front matter © 2004 Published by Elsevier B.V.
doi:10.1016/j.margeo.2004.11.008

1. The geological setting of the 1975 Kalapana event

The Kalapana earthquake of November 29, 1975 is the second largest historically recorded earthquake to have affected Hawaii, after the slightly larger Great Kau earthquake of 1868 (Brigham, 1909; Wyss, 1988). It produced a substantial tsunami, responsible for two deaths, and large-scale ground deformation of the south flank of Kilauea volcano (Tilling et al., 1976). This deformation was observed onshore, and is inferred to have extended offshore to produce the tsunami. Explanations of the tsunami and of the ground deformation have been principal objectives of subsequent investigations of this event (e.g., Ando, 1979; Ma et al., 1999). In this paper, we constrain three distinct tsunami sources by combining (i) a structural interpretation of geological data with (ii) modeling of the tsunami using recent seismic analyses. In the process, we endeavor to synthesize known onshore and offshore geological data in an inclusive and uncontroversial manner.

Our objective is to produce a mechanically realistic model for the 1975 Kalapana event, one that places this event in the context of the overall deformation and geological evolution of the south flank of Kilauea. We acknowledge that much of the sequences of rock underlying this flank may have originated from Mauna Loa (Lipman et al., 2002). Nevertheless, we consider that much of the deformation that took place during the 1975 Kalapana event is a result of the growth of Kilauea volcano and its rift zones (see Wyss, 1988, for exemptions). Since we are concerned with the deformation and evolution of a specific volcano flank, we continue to refer to it as the south flank of Kilauea, for the purpose of identification.

Eyewitness accounts of wave activity (summarized in Table 1) from the campsite at Halape (see Fig. 1) indicate that the 1975 Kalapana event had multiple tsunami sources. Immediately after the earthquake, some 10 to 60 s after ground shaking diminished the sea level at Halape began to rise. Within a minute this rise accelerated into a breaking, surging elevation wave some few meters high. Several minutes later, the observers were overwhelmed by a second wave, with an elevation that attained 7.0 to 14.6 m above sea level along this part of the coast. At Punaluu, 30 km southwest of Halape, the first wave also arrived within a few minutes of the end of the earthquake and was followed some 10 min later by larger waves. At greater distances from Halape, such as at Hilo, and along the western coast of the island of Hawaii, more conventional wave trains with growing and decreasing amplitude envelopes were recorded.

Table 1
Critical eyewitness observations of the 1975 Kalapana tsunami

Time	Observation
End of main stock	No immediate sea withdrawal
10–60 s after main stock	Rapid water rise and rushing wave
Shortly after first wave	Second wave of similar amplitude
Several minutes later	Withdrawal of the sea
After catching their breath	Much larger, turbulent wave attack
After largest wave attack	Several smaller elevation waves

Observations are taken from Tilling et al. (1976).

Onshore ground deformation associated with the 1975 earthquake was also most intense in the area around Halape, rather than in the epicentral area around Kalapana, some 25 km to the east (Tilling et al., 1976; Lipman et al., 1985). Up to 3.5 m of subsidence and 8 m of lateral displacement occurred around Halape, in an area extending from the Hilina–Holei fault scarps to the coast, but only some 15 km long in an east–west direction (Fig. 2b). Lesser amounts of subsidence and lateral displacement, typically around 1 m in magnitude, occurred in a more elongated region extending along the coast from the Halape area to east of Kalapana. There are some indications that subsidence was greatest just inland from the coast: coastal sites at Kaena Point and Kalapana subsided less than adjacent sites inland (Fig. 2a). Subsidence also occurred in an area to the north, extending from Kilauea caldera to the Kaoea faults (Fig. 2b). This vertical deformation was accompanied by south-directed horizontal displacement, with extension increasing from Kilauea caldera and the volcanic rift zones to the coast, and from east to west reaching a maximum in the coastal area around Halape. Despite this widespread deformation, actual ground ruptures along major onshore faults were limited to the western end of the Hilina–Holei fault system in the Halape area, and to the Koae faults and Kilauea caldera. As much as 2 m of horizontal extension occurred across the Koae fault system. At Kilauea caldera itself, dyke emplacement and a brief fissure eruption also took place in the hours after the earthquake (Tilling et al.,

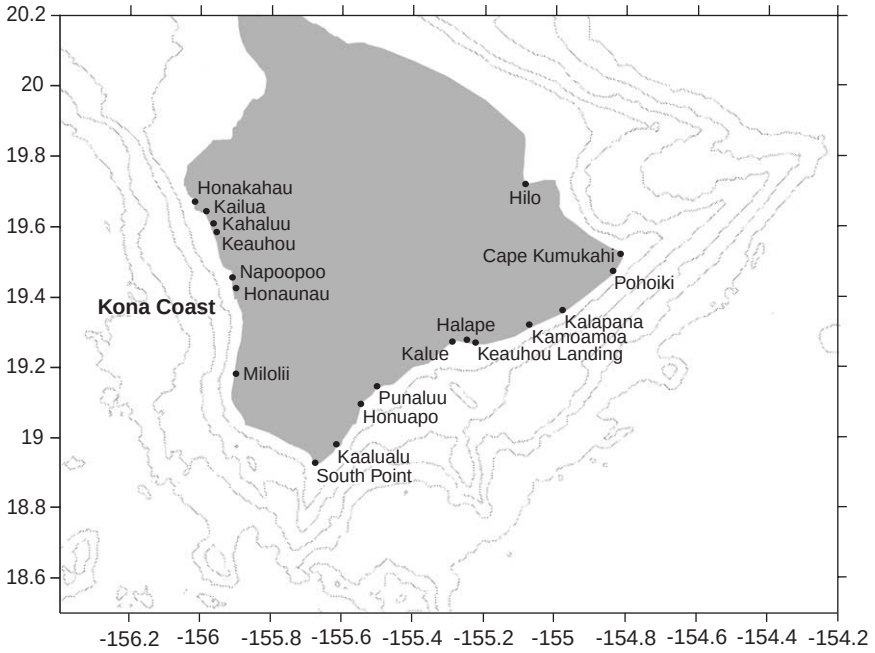

Fig. 1. Location map of Hawaii, showing some of the sites at which the 1975 Kalapana tsunami was observed. The map also provides the degrees latitude and degrees longitude of the uniform 400 m simulation grid. Bathymetric contours occur every 1000 m.

1976) providing further evidence of extension along the volcano flank.

Large faults and slump structures must from over time, presumably through small slip events followed in time by larger slip events. This phenomenon is well documented for faults (Wells and Coppersmith, 1994) and also appears to be the case for incipient landslide structures (Muller and Martel, 2000). Consequently, large total displacements, with or without substantial earthquakes. A corollary of this is that the structures responsible for the 1975 Kalapana event, unless continuously buried by sedimentation or by accumulation of lava flows, should be evident in the onshore topography and offshore bathymetry of Kilauea. Even if these structures are buried, they could appear in geophysical surveys of structures, under favorable conditions.

Recent multibeam and backscatter surveys (Smith et al., 1999) and seismic profiling (Morgan et al., 2000, 2003; Hills et al., 2002) of the south flank of Hawaii provide insight into the detailed structure of this region. Fig. 2a shows uninterpreted bathymetric data from Smith et al. (1999), while Fig. 2b shows major structural features identified by these authors, in addition our proposed north-facing fault structure (Lipman et al., 1985) or a deep thrust fault (Thurber and Gripp, 1988). The tsunami generation mechanisms proposed in each of these studies are likely to play a role in a more complex tsunami generation sequence. Recent studies of the 1994 Skagway, Alaska event (Thomson et al., 2001) and the 1998 New Papua Guinea event (Tappin et al., 1999, 2001, 2002, 2003; Watts et al., 2002, 2003) have considered multiple tsunami sources as part of complex geological structures, in the case of Papua New Guinea both faulting and mass failure. We will use the geological studies of Kilauea, to identify multiple structures that may have been involved in the 1975 Kalapana event.

1.1. Three tsunamigenic structures

The occurrence of the first wave at Halape immediately after the earthquake (see Table 1) is in our view a critical feature of the tsunami. It requires an area of localized subsidence, as observed by a region of reduced subsidized or even uplift further offshore. To explain this observation, we

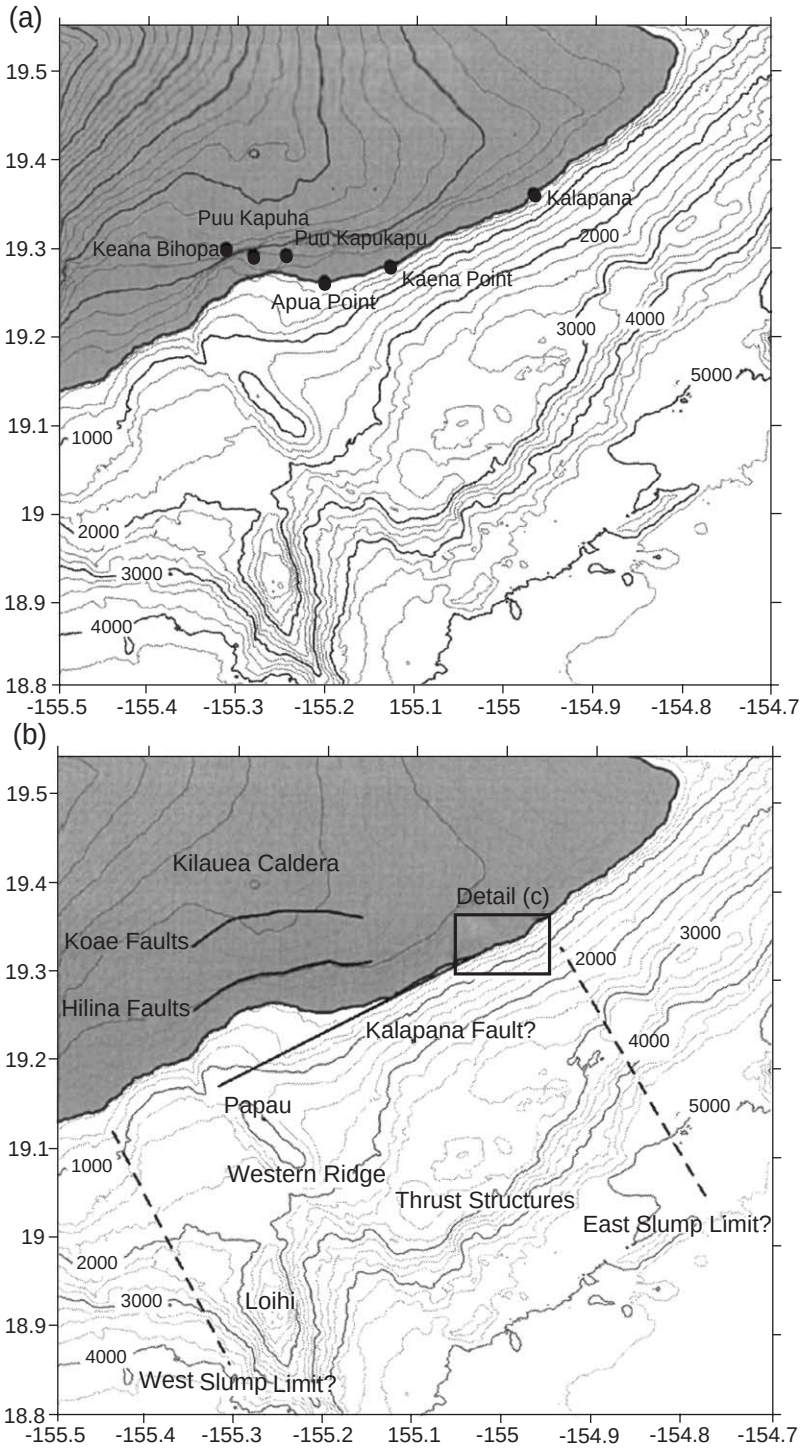
(a)
Kalapana
Puu Kapuha
Puu Kapukapu
Keana Bihopa
Kaena Point
Apua Point
2000
3000
4000
5000
1000
19.5
19.4
19.3
19.2
19.1
19
18.9
18.8
-155.5
-155.4
-155.3
-155.2
155.1
-155
-154.9
-154.8
-154.7
(b)
Kilauea Caldera
Detail (c)
Koae Faults
Hilina Faults
Kalapana Fault?
Papau
Western Ridge
Thrust Structures
East Slump Limit?
Loihi
West Slump Limit?

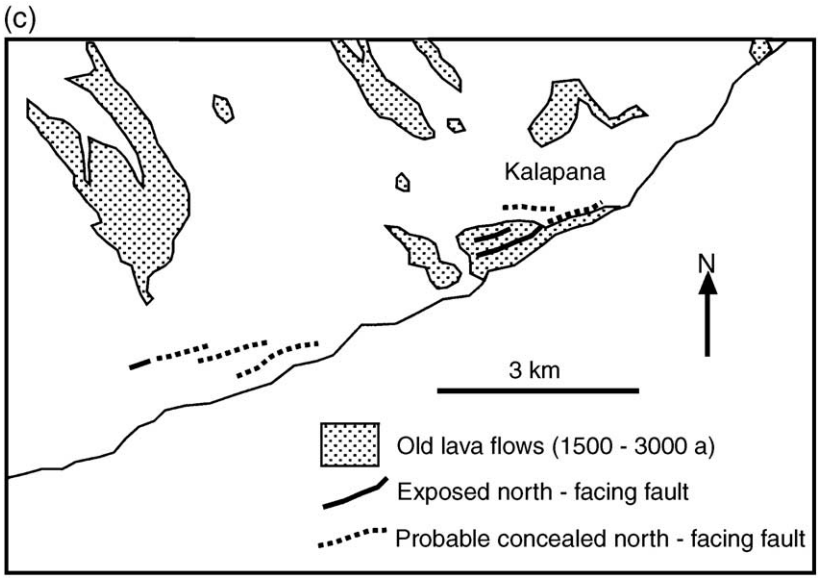

Fig. 2. (a) Uninterpreted contours of the southern flank of Kilauea volcano mapped as degrees latitude and degrees longitude with bathymetric contours in meters (courtesy of John Smith). (b) Structural interpretation of the same area (modified after Smith et al., 1999). (c) Detail showing north-facing faults in the Kalapana area that depict a correlation between exposure of faults and exposure of old basalts (simplified from Wolfe & Morris, 1996).

infer movement on a north-facing fault structure running broadly parallel to the coast and offshore of Halape that we name the Kalapana fault. Two other structures further offshore are required to account for (i) the larger second elevation wave at the Halape and (ii) tsunami observations made at greater distances, respectively. Evidence for all three tsunamigenic structures is present in the geological record. The spatial relationship of the Kalapana fault and of previously known geological structures is outlined in Fig. 3. We consider the three tsunamigenic structures in turn:

1. Our proposed Kalapana fault is a north-facing, landward-dipping normal fault situated just offshore and extending along the coast from Kalapana to Kalue (Fig. 2b) To the west of Apua Point (Fig. 1), we propose that the fault forms the southern boundary of an area south of Halape where the seafloor slopes gently southwest,

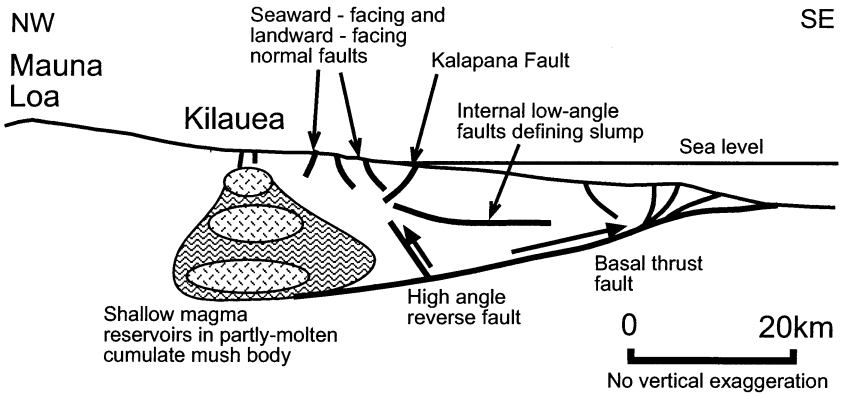

Fig. 3. Schematic cross-section showing previously identified geological structures that were potentially active during the 1975 Kalapana event.

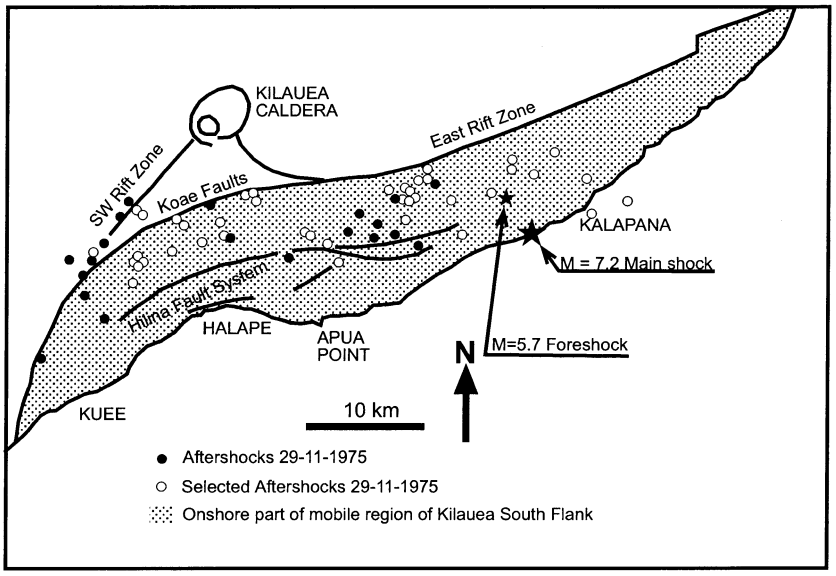

Fig. 4. Seismic constraints on the 1975 earthquake from foreshock and main shock epicenters as well as aftershock distribution (modified after Tilling et al., 1976).

suggesting a ramp linking the north to Kalapana fault to the southwest-facing Hilina faults to the north and west (Figs. 2b and 4). East of Apua point, we proposed that the remarkably flat ground between the Hilina–Holei escarpments that the coast contains the concealed graben structure that have been filled by lava flows. We note that back rotation of hanging wall blocks on curved Hilina–Holei faults (Riley et al., 1999; Cannon et al., 2001) could account for some aspects of the geometry of this region. However, this does not explain the extensive subsidence along the coast east than the eastern limit of Hilina–Holei escarpments that developed in 1975 (Lipman et al., 1985). We acknowledge that an antithetic fault internal to volcano flank slumping is also consistent with tsunami observations and offshore normal faulting, but we argue that Kilauea flank mobility to runs too deep, extends too wide, and is expressed too prominently for such an interoperation. In the end, such distinction may be semantic in nature because the mechanical actions responsible for the Kalapana fault may be similar to those responsible for antithetic faulting within a slump (see Yin and Kelty, 2000).

2. A large slump structure occupies the region between the coast and the zone of ridges at around 3000 m depth (Fig. 2a), and even larger slump structures may extend from Hilina Pali all the way to thrust complexes near the volcano toe. Morgan et al. (2000, 2003) and Hills et al. (2002) identify a series of imbricated (in the southwest) to stacked (in the northeast) structures that form the ridges from thrust structures at around 3000 m/depth. The western boundary of this region is coincident with the uplifted and highly deformed area of the western ridge (Fig. 2b). The eastern boundary of this region is not evident in the seafloor topography, because of high sedimentation rates on the upper flank and midslope bench areas, but can be inferred from the transition from imbricated to stacked-thrust deformation structures in the multiple seismic lines of Morgan et al. (2000) and Hills et al. (2002). The upslope limit of the overall slump structure is less well defined. Lipman et al. (1985) propose that the Hilina–Holei faults represent the headwall of slump that moved in 1975. More recent studies (Riley et al., 1999; Parfitt and Peacock, 2001) indicate that the Hilina faults are deep-seated structures, although this does not exclude the possibility that individual episodes of movement on their near-surface sections can be related to slump events; perhaps as control faults. Within the slump region itself, one or more slump

masses may be included or layered such that each moved by different amounts in 1975. However, the available information does not allow us to identify movements on substructures within the general region of the slump, and so we treat the slump as single coherent structure.

3. Faults exist in the toe thrust complex identified by Smith et al. (1999) beneath the outer scarp region at the seaward limit of the south flank of Kilauea (Fig. 2b). In this region, the low-angle basal detachment developed at the interface between the Hawaii volcanic edifice as a whole and the underlying oceanic crust steepens into a thrust duplex as it approaches the surface (Morgan et al., 2000, 2003; Hills et al., 2002). Movements on the basal detachments of the seafloor will therefore result in vertical displacements that are intrinsic to the thrust structures, as opposed to the slump itself. Consequently, the thrust complex is a distinct tsunami source that can contribute considerable wave potential energy.

Hyaloclastite debris lobes from lava flows occur extensively offshore (Smith et al., 1999) and are inferred to cover any surface scarp generated by the Kalapana fault. This situation is comparable to that of the north-facing Koae faults onshore, shown by Parfitt and Peacock (2001) and Peacock and Parfitt (2002) to be much larger and long-lived structures than their present surface rupture displacements would indicate. We argue that the Kalapana fault has not previously been recognized as a large-scale structure because its north-facing geometry makes it susceptible to burial by lavas and hyaloclastites. There are a few places along the south coast of Kilauea where north-facing faults are exposed onshore (Fig. 2c). East of Kalapana, north-facing normal faults form the southern boundary of an area of localized subsidence in 1975 (Tilling et al., 1976). Other such faults were exposed at the coast west of Kalapana in an area now covered by lavas of the ongoing Pu'u Ou'u eruption (Wolfe and Morris, 1996). These onshore faults may represent splays from the Kalapana fault towards its eastern termination. Their onshore location near Kalapana provides the fault name.

Recent seismic reflection studies (Hills et al., 2002; Morgan et al., 2003) appear to provide evidence of the Kalapana fault. Most of the seismic lines described in these studies end further offshore than the position of the proposed Kalapana fault, with the exception of their lines 14 (SW–NE) and 15 (NW–SE), which both pass over the prominent break or scarp in the submarine slope south of Halape (Fig. 2a). We consider that this prominent feature defines the southwestern end of the Kalapana fault (see Fig. 1 of Morgan et al., 2003). The fault itself is not directly imaged in the seismic lines, but as noted by Morgan et al. (2003) this is to be expected for steeply dipping fault structures. In general, seismic data can only be used to rule out geological structures. The Kalapana fault appears to break the surface near shot point 400 in line 14 (Fig. 6 of Morgan et al., 2003) and below shot point 100 in line 15 (Fig. 7 of Morgan et al., 2003). This suggests the presence of a structural transition more or less coincident with the south coast of Kilauea, one that may even control the location and shape of the coastline.

Surface rupture on the Hilina faults in 1975 is restricted to the western end of their outcrop, with maximum seaward displacement along the coast on the order of 8 m. Cannon et al. (2001) argue that this displacement at the coast is too great to be accounted for by seismic slip on the basal thrust of the south flank of Kilauea and therefore argue for movement on a slump structure with its headwall at Hilina Pali as a component of the 1975 earthquake. However, as will be shown below, a slump displacement of some tens of meters is required to make significant contribution to the tsunami. The largest displacements of any such must therefore occur largely offshore, with extension between the slumped mass and the upslope limit of the headwall region being accommodated on a series of mostly offshore faults. Our proposed Kalapana fault may also be viewed as part of this system, and if it is comparable to the Koae faults it will extend to great depth within the volcano. This is suggested by the prominence of the offshore scarp.

Displacements on the proposed Kalapana fault, the slump, and thrust complex are coupled, allowing us to place geometrical constraints on the movement of the submarine slump from the onshore deformation, even though the main part of the slump is located offshore. Although the exact value of slump displacement required by the onshore subsidence depends on the dip angles of the basal surface and of the Kalapana

fault, the overall conclusion that the slump displacement must be much greater than the subsidence is required by the overall geometry of the coupled system. Movements of the toe thrust system are likewise constrained by a similar argument, and the magnitude of slip is constrained by a recent reanalysis of the seismic records of the 1975 Kalapana earthquake, discussed in Section 2 below.

Previous studies have typically modeled tsunami generation by one structure at a time, either an earthquake source or a slump source (e.g., Ando, 1979; Ma et al., 1999), although proposals that the 1975 Kalapana event involved both date back to at least Kawakatsu (1989). The need for multiple tsunami sources to accommodate geological complexity is not surprising (Watts, 2001). Our work differs from these earlier tsunami studies in two fundamental ways. On the other hand, we consider three tsunami sources, one from each of the geological structures that we identified above. This means that there are *two* earthquake sources and *one* slump source. On the other hand, we proceed with direct tsunami modeling based tsunami generation by each on of these structures. That is, we rely on our geological interpretation to provide tsunami source parameters that are then compared to tsunami observations and records. This clearly an iterative process, as we have used the tsunami observations to help identify the Kalapana fault in the first place. We point out that our geological interpretation and tsunami modeling stand on their own merits, by satisfying geological data and tsunami observations, respectively. Therefore, the iterative process does not represent a circular argument, but rather it furthers our fundamental understanding of complex volcano structures and tsunami events.

2. Seismic records of the 1975 earthquake

Numerous interpretations of the seismic records of the 1975 earthquake have been made, beginning with Ando (1979) and Furumoto and Kovach (1979). However, some regions of the south flank of Kilauea exhibit aseismic slip, including rapid slip events (Cervelli et al., 2002). Thus, while the seismic data is important in identifying structures that may have slipped as part of the 1975 Kalapana event, it cannot be used to exclude other structures that may be required to explain the geodetic or tsunami data. That is, the seismic data can confirm rupture along certain structures, but there can be additional ruptures and mass failures that remains seismically silent, perhaps on account of significant (i) water pressures within the volcano or (ii) alteration of volcanic sediments to produce clays. The magnitude of slip along a given fault derived from seismic records can only be expressed as a minimum, as additional *aseismic* slip could be present. The magnitude of slip is only constrained by geodetic data.

This situation has long been recognized with regard to the Hilina–Holei fault system. Slip on the western part of this fault system during the 1975 earthquake is well documented from the surface ruptures and ground deformation, but it did not provide an identifiable contribution to either the seismic records of the earthquake or to the aftershock population (Tilling et al., 1976; Lipman et al., 1985). This fault system is also a major contributor to the ongoing seismicity of the volcano (Denlinger and Okubo, 1995). Given these facts, the absence of seismicity associated with the Kalapana fault is not strong argument against either its existence or the proposal that it ruptured as part of the 1975 Kalapana event. This situation may in part reflect the early state of development of the seismic network on the volcano at that time. Aftershocks of the 1989 Royal Gardens earthquake (Bryan, 1992) include a number of events within a few kilometers of the surface, offshore from Kalapana, that may have occurred on our proposed Kalapana fault. Regardless, we supplement seismic analyses with a more mechanical model of volcano deformation and geological evolution in order to overcome this situation.

Two classes of structures have been inferred from the seismic data for the 1975 earthquake: high-angle faults and low-angle faults. Proposed dip values and dip directions have varied widely between the studies. The strike of the proposed faults has remained relatively stable (at around N70E) and slip has been inferred to be primarily dip-slip *until* the most recent study of Nettles and Ekstrom (2004). Given such uncertainty, seismic analyses deserve careful consideration.

2.1. High-angle faults

In the south flank of Kilauea, focal plane solutions related to movement on high-angle, steeply dipping faults emerge from studies of the short-period, high-frequency components of the seismic records (Bryan, 1992). Interpretation of these records is difficult because of the complex velocity structure between the earthquake sources and the seismometers (Lipman et al., 2000, 2002). Bryan (1992) suggests a seaward-dipping high angle reverse fault close to the coastline, with rupture beginning beneath Kalapana at a depth of as much as 10 km and propagating unilaterally westwards, as the source of both foreshock and the initial stage of the main shock itself (Fig. 4). In this interpretation, rupture extended into the low-angle faults beneath the flank of Kilauea at a later stage in the earthquake. The first-motion analysis of Ando (1979) also indicates a steeply dipping fault as one possible source of the initial stage of the earthquake record.

2.2. Low-angle faults

Focal plane solutions related to movement on low-angle, gently dipping faults or slump detachments generally emerge from studies of long-period teleseismic records of the earthquake. These indicate movement on near horizontal to NNW dipping thrust faults, generally identified with structures slipping along the basal interface between the volcanic edifice and the underlying sediments, or in a weak layer formed by the sediments themselves (Crosson and Endo, 1982; Thurber and Gripp, 1988; Got et al., 1994), or on SSE dipping surfaces identified as the basal surfaces of slumps within the flank of Kilauea volcano (Swanson et al., 1976; Lipman et al., 1985; Eissler and Kanamori, 1987). The source of the seismic energy has been identified as a region some 60 km long and only 20 km wide, extending WSW from Kalapana and broadly coincident with the region of aftershocks (Fig. 4). It has long been recognized that this proposed source region is landward of the inferred locations of the tsunami source (Ando, 1979; Ma et al., 1999) and the usual resolution has been to propose that only the landward part of the fault rupture generated seismic waves, with aseismic slip further offshore.

However, a recent reanalysis of the long-period seismic records has resulted in a different fault plane solution and seismic source location (Nettles and Ekstrom, 2004). This study places the epicenter of the long-period seismic energy further offshore and around 70 km to the southwest of the Kalapana, at the southwestern end of the toe thrust complex. The orientation and slip geometry of the proposed fault is also different from the results of the earlier studies: a SW-directed, oblique-slip thrust event. This is consistent with the geological structure of this area (Fig. 2b). The Nettles and Ekstrom (2004) location for the long period seismic source makes it suitable candidate for the third tsunami source in the scheme outlined above. The Southwest end of the toe thrust complex is at the opposite end of the deforming part of the south flank from the earthquake hypocenter beneath Kalapana. The rupture process probably ended in this part of the toe thrust complex, with deformation of the sea floor occurring towards the end of the seismic activity.

3. Simulation results for the 1975 Kalapana tsunami

Our interpretation of the geological setting is subject to direct numerical simulations. In this case of the 1975 Kalapana event, tsunami observations provide significant constraints of tsunami sources as well as on some of the fundamental geological phenomena. Kilauea volcano presents various local regimes of extension and compression in order to compensate for volcano deformation. We choose three tsunami sources that capture the most tsunamigenic geological phenomena, and that provide a mechanically consistent description of the 1975 Kalapana event. We also choose a tsunami propagation and inundation model that is sufficiently accurate for the results to be compared directly with actual tide gauge records. The level of accuracy of geological interpretation, tsunami sources, and propagation results will turn out to be commensurate with each other and with all available tsunami observations and records. The caveat is that our tsunami sources remain poorly constrained for a lack of geological data, with consequences on tsunami results that we discuss in Section 4 below.

3.1. Methodology

Version 1.2 of the "Tsunami Open and Progressive Initial conditions system" (TOPICS) provides the earthquake and slump tsunami sources in our work. For vertical coseismic displacement, TOPICS is based on the half-plane solution of an elastic dislocation problem (Okada, 1985). A planar fault of length L and width W is discretized into many small trapezoids and the point source solution of Okada (1985) is used to sum the contributions made by each trapezoids to vertical coseismic displacement, based on the actual depth of the trapezoid. The shear modulus μ can be specified based on the depth of the earthquake centroid as well as other seismic and geological descriptors. TOPICS outputs a characteristic wavelength λ_0 that is the smaller of the fault dimensions L or W, and a characteristics tsunami amplitude η_0 that is the minimum depression found from the coseismic displacement. The seismic moment M_0 is proportional to but slightly less than $\mu LW\Delta$ because a Gaussian slip distribution is assumed about the centroid, where Δ is the maximum slip. TOPICS allows for the superposition of multiple fault planes, which can be assembled into complex fault structures or slip distributions.

For underwater slumps, the initial free surface elevation *and water velocities* in TOPICS were derived from multivariate, semi-empirical curve fits as a function of non-dimensional parameters characterizing the landslide (e.g., density, geometry, etc.) and the local bathymetry (e.g., slope, depth, etc.). Water velocities are new to version 1.2 of TOPICS. Relevant non-dimensional parameters were selected based on the scaling laws of Watts (1998, 2000). Numerical experiments were carried out first with the 2D model of Grilli and Watts (1999) and the curve fits were then modified based on results from a more recent 3D model (Grilli and Watts, 2001; Grilli et al., 2002). The curve fitting approach that led to TOPICS was initially proposed by Grilli and Watts (1999), applied by Goldfinger et al. (2000), and reported in Watts et al. (2003). The duration of landslide acceleration t_0 in the numerical simulations is also the duration of tsunami generation (Watts, 1998; Watts and Grilli, 2003). Consequently, TOPICS provides a slump initial condition at time $t=t_0$, as if results from the models of Grilli and Watts (1999) or Grilli et al. (2002) were being transferred directly to the tsunami propagation model at that instant of time. Researchers can find more information on TOPICS or request a free copy of TOPICS software from the web site www.tsunamicommunity.org.

We simulate tsunami propagation and inundation with FUNWAVE, a public domain Boussinesq water wave model developed at the University of Delaware (Wei and Kirby, 1995; Wei et al., 1995; Chen et al., 2000; Kennedy et al., 2000). FUNWAVE is a fully nonlinear Boussinesq model retaining information to $O((kh)^2)$ in frequency dispersion and to all borders in nonlinearity a/h, where k denotes an inverse wavelength scale, a denotes a wave amplitude, and h denotes a water depth. Wei et al. (1995) have demonstrated that the retention of nonlinear effects beyond the usual ordering in weakly nonlinear Boussinesq models is crucial to the correct modeling of shoaling solitary wave crests, and thus is important in the modeling of shoreline inundation. The presence of frequency dispersion in the model is important for the case of short wave propagation into relatively deep water, and allows for the mechanism of wave crest splitting during wave propagation over shallow bathymetry. FUNWAVE includes dissipation from breaking waves, and model predictions of shoreline runup have been well tested in the case of short wave shoaling and breaking.

We combine TOPICS and FUNWAVE into a single model referred to as Geowave, in which the tsunami sources predicted by TOPICS are transferred as initial conditions into FUNWAVE. Geowave can simulate multiple tsunami sources with different generation mechanisms, occurring at different times. The new software needed to manage multiple tsunami sources is one reason for the name Geowave. The benefits of a Boussinesq wave propagation model over traditional nonlinear shallow water wave models is that the horizontal velocity profile over depth is no longer constrained to have a constant value, and vertical accelerations (i.e., non-hydrostatic pressures) are no longer neglected. Dispersive effects are both necessary and manifested during propagation of deep water waves, during propagation of an undular bore, and during propagation of edge waves (Liu et al., 1998). Geowave has been validated based on case studies of a pyroclastic flow generated tsunami (Waythomas and

Watts, 2003) and several underwater landslide generated tsunamis (Watts et al., 2003; Fryer et al., submitted for publication). Geowave has also been applied to a debris flow generated tsunami (Walder and Watts, 2003). Despite this prior work, the 1975 Kalapana event remains perhaps the most difficult case study using Geowave to date.

3.2. Derivations of three distinct tsunami sources

We begin our derivation of the three tsunami sources with the observation that the region around Halape subsided by around −3.0 m during the 1975 Kalapana event. Our Kalapana fault tsunami source must be able to reproduce this local observation, which serves as the mechanical anchor for the two other tsunami sources. We restrict the Kalapana fault source to the region immediately offshore the largest deformations, as we have reason to believe that slip is more pronounced in this region. That is *not* to say that slip failed to occur elsewhere along the Kalapana fault, as it almost certainly did, only that such slip is significantly less than the slip we expect off Halape, due to the large local extension. The hypocenter, width, length, and strike of the Kalapana fault source are constrained by the local volcano thickness, the region of largest Kilauea deformation, and the lineament formed by the shoreline west of Kalapana itself. For simplicity, we assume a purely normal fault mechanism with a typical dip of $\delta \cong 60^\circ$. The slip needed to produce the observed subsidence around Halape is $\Delta \cong 11.4$ m, a magnitude of slip that is consistent with known displacements in that region. Water pressures within Kilauea may have played an important role facilitating such a large aseismic slip. We neglect coseismic displacement from onshore faults given their smaller slip and distance from the shoreline. The resulting Kalapana fault source parameters are summarized in Table 2.

Table 2
Kalapana fault tsunami source parameters

Quantities	Kalapana
x_0 (longitude)	−155.24°
y_0 (latitude)	19.23°
d (km)	5.2
φ (°)	60°
λ (°)	90°
δ (°)	60°
Δ (m)	11.4
L (km)	22
W (km)	12
μ (Pa)	4×10^{10}
M_0 (J)	9.6×10^{19}
λ_0 (km)	12
η_0 (m)	−5.1

The input for TOPICS are, in descending order, the longitude of the earthquake centroid x_0, the latitude of the earthquake centroid y_0, the centroid depth d, the fault strike counterclockwise from north φ, the fault rake clockwise from strike λ, the fault dip δ, the maximum slip Δ, the fault length along rupture L, the fault width across rupture W, and the shear modulus μ. The outputs from TOPICS are the seismic moment M_0, the characteristic wavelength λ_0, and the characteristic tsunami amplitude η_0. The opposite convention yields strike 240° and rake 270°.

We derive the slump source in part from the Kalapana fault source. The slip inferred on the Kalapana fault constrains the distance of slump motion $2s_0$ along a mean failure plane of $\theta \cong 6.3^\circ$. In order to maintain the integrity of the volcano flank, continuity of several displacement suggests the equation $\Delta \sin\delta \approx 2s_0 \sin\theta$ that yields a distance of slump motion $2s_0 \cong 90$ m. This distance of slump motion applies primarily near the center of mass, because the slump is foremost in extension, with less motion near the headwall and more motion near the center of mass, as observed on land from Kilauea caldera to the shoreline. Given the $b \cong 60$ km distance from Hilina Pali to the approximately 5000 m deep toe of Kilauea, it is clear that the major portion of the slump is submarine, and that the displacements measured on land can be expected to be a small fraction of the maximum slump motions. The slump maximum thickness $T \cong 6$ km is intended to represent mass failure down to the oceanic crust interface, because we expect the structural evolution of Kilauea to involve the entire southern flank. This assumption does not exclude slip within the slump mass proper, similar to mass failures described by Morgan et al. (2003), which would enhance both slump extension as well as tsunami generation. The width of large slumps is often found to be similar to slump length $w \cong b$, and the flank of Kilauea is no exception. The width $w \cong 60$ km corresponds to the entire active flank of Kilauea, as demonstrated by offshore thrust structures visible in the bathymetry (Fig. 2b), and by coseismic displacement from the thrust fault tsunami source (see Section 3.3 or Fig. 5e). We assume an

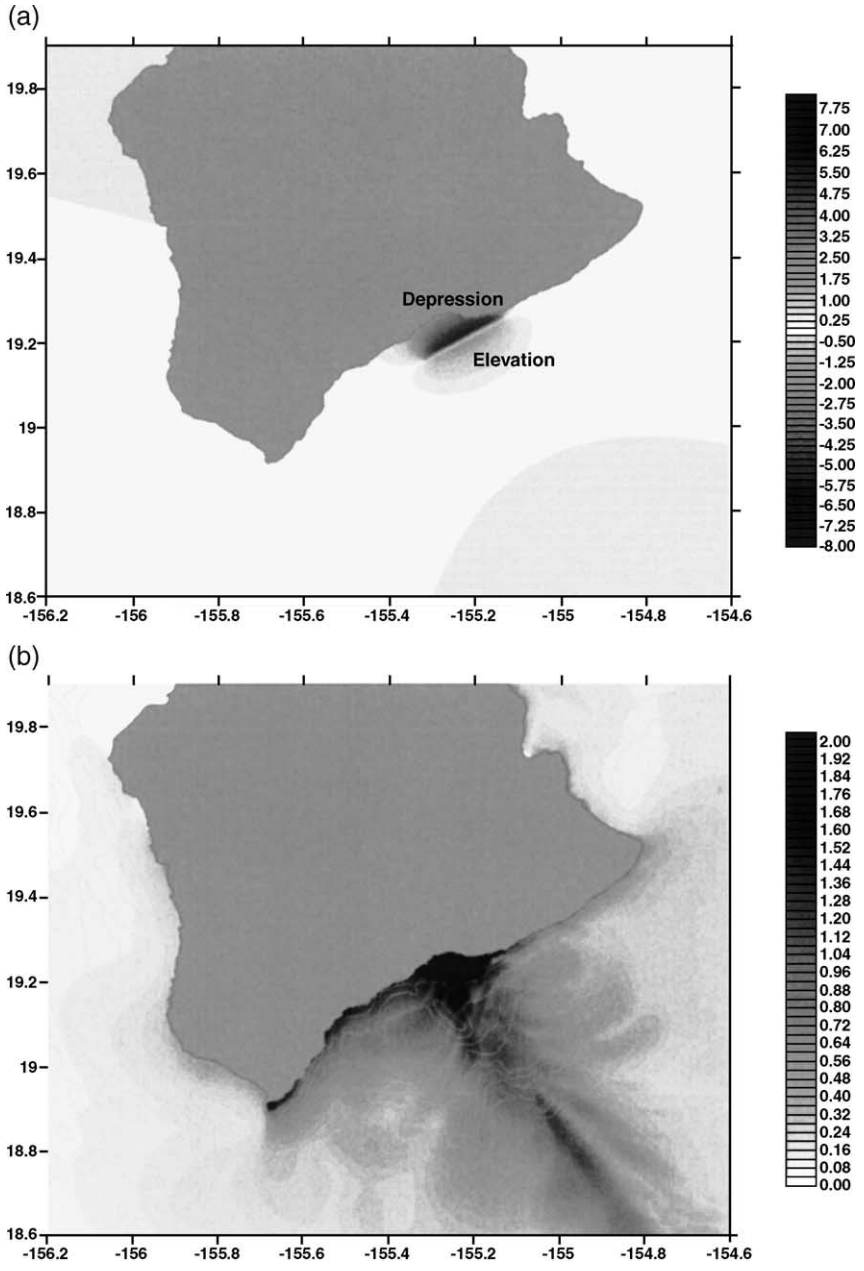

Fig. 5. The three tsunami sources inferred in this study considered independently: (a) Kalapana normal fault initial condition in meters, (b) simulated maximum wave elevation above sea level in meters, (c) Kilauea flank slump initial condition in meters, (d) simulated maximum wave elevation above sea level in meters, (e) basal thrust fault initial condition in meters, and (f) simulated maximum wave elevation above sea level in meters. See the text for a discussion of discrepancies between each source treated independently versus the combined sources shown below (Fig. 8).

average volcano flank density of ρ_b=2800 kg/m^3. The resulting slump source parameters are summarized in Table 3.

We show that the oceanic crust interface provides a weak surface along which mass failure of the entire south flank of Kilauea can occur. The tsunami source

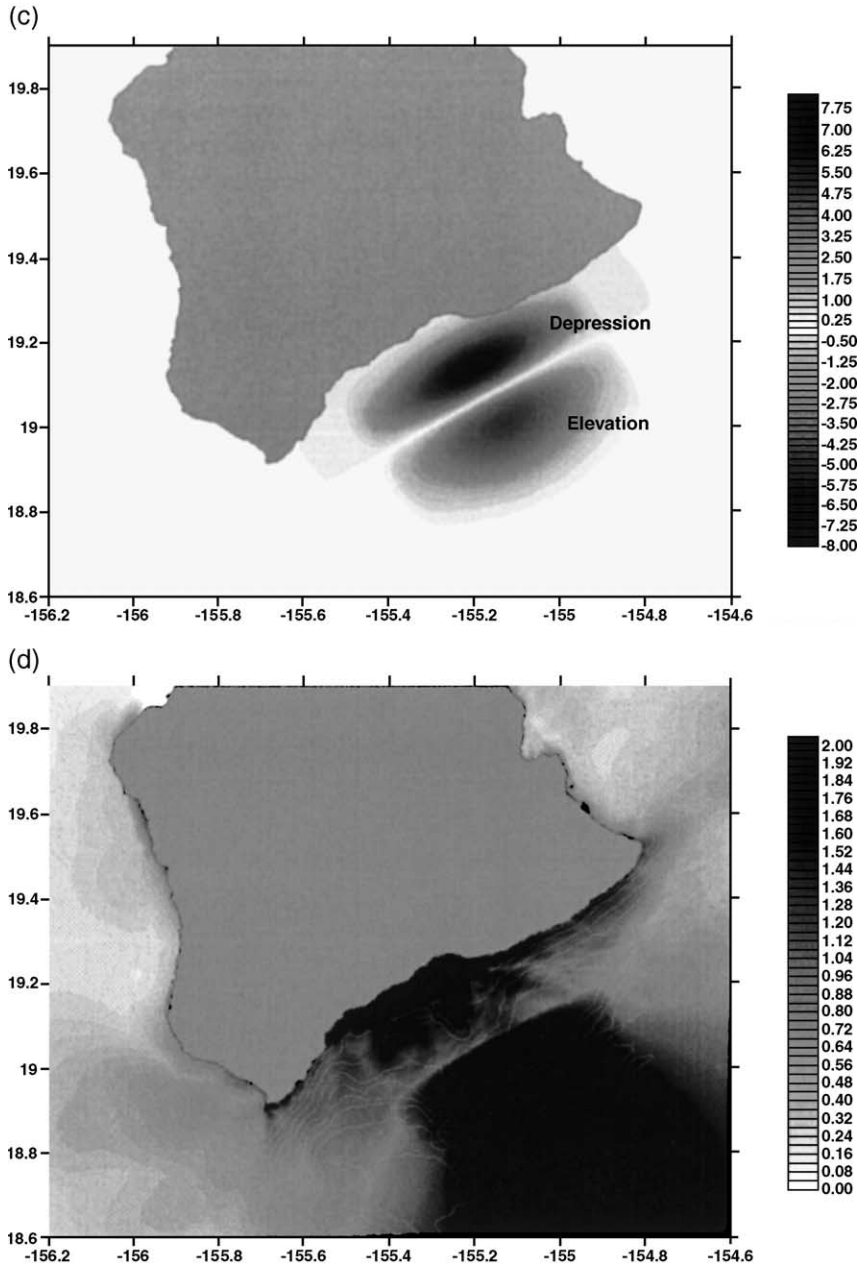

Fig. 5 (*continued*).

information in Table 3 includes the characteristic distance of slump motion s_0 and the characteristic time of slump motion t_0, which serve to define slump motion according to $s(t)=s_0[1-\cos(t/t_0)]$ valid for times $0<t/t_0<\pi$. This motion was part of the original 2D and 3D numerical model experiments and therefore remains implicit to TOPICS slump tsunami sources (see Watts et al., 2002, 2003). The characteristic distance of slump motion s_0 also constrains the typical shear stress $\tau \approx 4Tg(\rho_b-\rho_0)s_0/9R$ along the

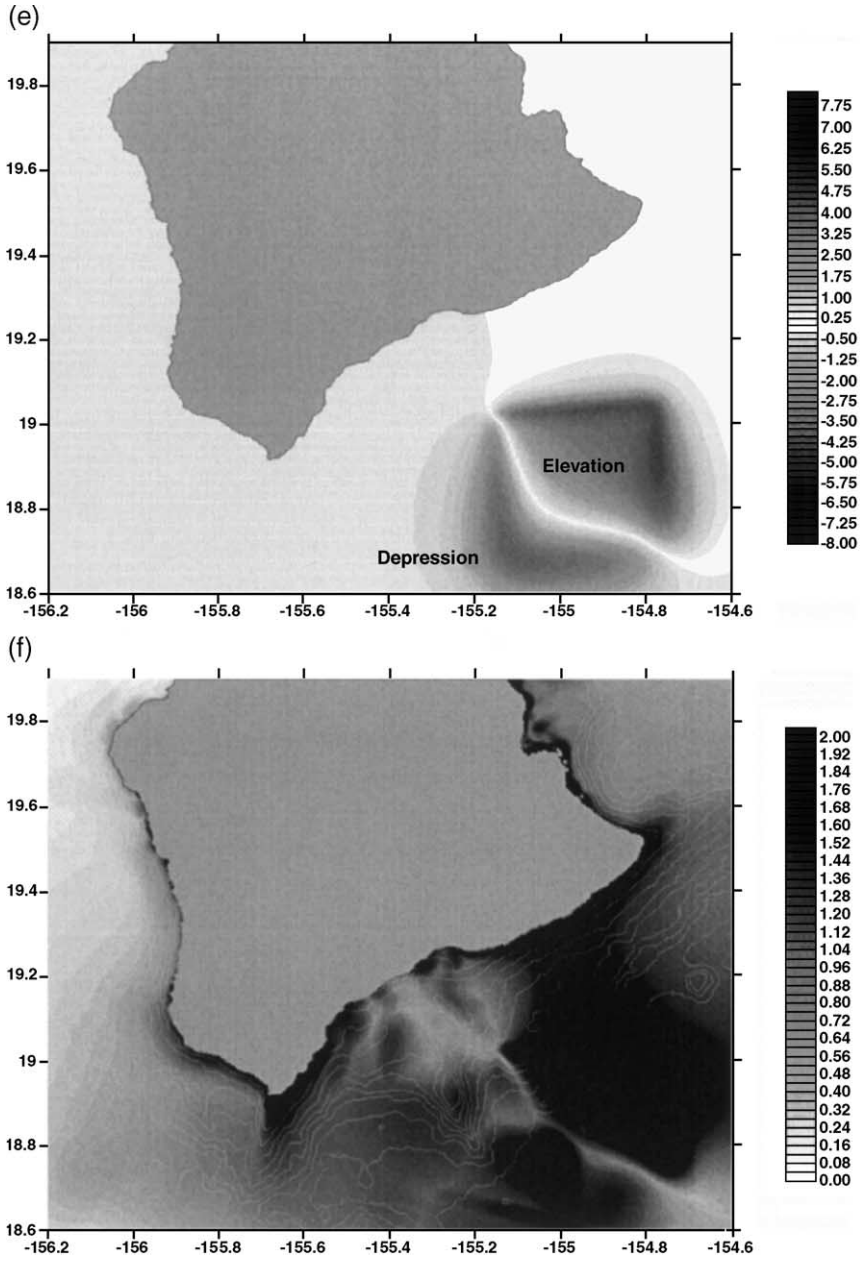

Fig. 5 (*continued*).

basal slip surface, where g denotes the acceleration of gravity, ρ_0 denotes the sea water density, and $R \approx b^2/8T$ denotes an approximate radius of curvature of the slump failure plane (Watts, 2004). We find a typical shear stress of around $\tau \approx 30$ kPa along the oceanic crust interface, which is surprisingly small given the size and overburden of Kilauea volcano. Alternatively, one could infer that the extremely small angular displacement of the slump, in this case $\Delta\phi \equiv 2s_0/R \cong 0.001$ radians, requires exceptional water pres-

Table 3
Slump tsunami source parameters

Quantities	Slump
x_0 (longitude)	−155.21°
y_0 (latitude)	19.14°
γ	2.73
b (km)	60
T (km)	6
w (km)	60
d (m)	1300
θ (°)	6.3°
a_0 (m/s^2)	0.0026
u_{max} (m/s)	0.34
s_0 (m)	45
t_0 (s)	131
λ_0 (km)	31.8
η_0 (m)	−5.8

The inputs for TOPICS are, in descending order, the longitude of the initial slump center x_0, the latitude of the initial slump center y_0, the specific density γ, the initial landslide length b, the maximum initial landslide thickness T, the maximum landslide width w, the mean initial landslide depth d, and the mean initial incline angle θ. The outputs from TOPICS are the slump initial acceleration a_0, the theoretical maximum slump velocity u_{max}, the characteristic distance of slump motion s_0, the characteristic time of slump motion t_0, the characteristic wavelength λ_0, and the characteristic tsunami amplitude η_0 from the depression wave at time $t=t_0$.

sures in order to reduce effective stresses to levels that permit mass failure (Watts et al., 2003). A more sophisticated study of basal shear stress also inferred exceptional water pressures along the volcano basal decollement (Yin and Kelty, 2000).

The thrust fault source is described almost completely by the seismic inversion work of Nettles and Ekstrom (2004). We decreased the fixed hypocenter depth of $d \cong 10$ km down to $d \cong 6$ km in order to place the earthquake at the base of the thrust structures, which presumably matches quite closely the 6 km thickness of the slump. The *minimum* possible earthquake slip is bounded by the $\Delta \cong 7.9$ m slip proposed by Nettles and Ekstrom (2004). However, such a small amount of slip is incommensurate with the distance of slump motion $2s_0$, and some of the thrust fault slip can be assumed to be aseismic. The *maximum* possible earthquake is bounded by the equation $2s_0 \sin\theta \approx \Delta \sin\delta$ that yields a slip $\Delta \cong 63$ m. We expect this slip to be too large because the thrust structure is in local compression, with significant vertical deformation taking place instead of horizontal motion. Any amount of slip between these two bounds is possible, and we choose an intermediate value of $\Delta \cong 25$ m with the understanding that the amplitude of this tsunami source is poorly constrained. The resulting thrust fault source parameters are summarized in Table 4.

We need to explain why the thrust complex should be included as a separate tsunami source, because slump motion and thrust slip are presumably mechanically interconnected. Tsunami generation by the slump originates from a loss in slump potential energy and occurs over the entire slump surface. Tsunami generation by the thrust complex occurs through the release of elastic energy and is confined to the region of thrust faulting near the toe. The two structures are therefore energetically and geologically distinct, despite being mechanically connected. We believe that the thrust complex provides a local constraint on the advancing toe of the slump. Therefore, slump motion could increase stresses within the thrust complex to the point of rupture. Case studies of the 1946 Unimak, Alaska and 1998 Papua New Guinea tsunamis suggest that landslide displacement triggered after shocks in the region immediately below mass failure (Fryer et al., submitted for publication; Tappin et al., 2001).

Table 4
Thrust fault tsunami source parameters

Quantities	Thrust
x_0 (longitude)	−154.95°
y_0 (latitude)	18.86°
d (km)	6
φ (°)	266°
λ (°)	313°
δ (°)	9°
Δ (m)	25
L (km)	40
W (km)	40
μ (Pa)	4×10^{10}
M_0 (J)	2.8×10^{21}
λ_0 (km)	40
η_0 (m)	−8.9

The inputs for TOPICS are, in descending order, the longitude of the earthquake centroid x_0, the latitude of the earthquake centroid y_0, the centroid depth d, the fault strike counterclockwise from north φ, the fault rake clockwise from strike λ, the fault dip δ, the maximum slip Δ, the fault length along rupture L, the fault width across rupture W, and the shear modulus μ. The outputs from TOPICS are the seismic moment M_0, the characteristic wavelength λ_0, and the characteristic tsunami amplitude η_0. The opposite convention yields strike 86° and rake 47°.

One explanation is that stress changes near existing faults can apparently trigger earthquakes (Stein, 1999). In general, reservoir filling of emptying as well as oil and gas production activities are also known to trigger earthquakes (Guha, 2001). The foregoing examples of earthquake triggering are mechanically indirect when compared to the *direct* bulldozer effect of slump motion pushing against the thrust complex.

3.3. Simulation results for three distinct tsunami sources

We simulated each tsunami source separately in order to better understand their respective wave activity. Our simulation of the 1975 Kalapana tsunami, carried out with the combined tsunami sources, is presented in Section 3.4. As a first approximation, the combined simulation can be viewed as a linear superposition of the three simulation presented in this section, given the typical water depths, wave amplitudes, and wavelengths found here. Consequently, the simulation results of each individual tsunami source contain valuable lessons that will inform our understanding of the 1975 Kalapana tsunami and of Kilauea deformation. These results will also demonstrate why three tsunami sources are necessary.

Fig. 5a illustrates the vertical coseismic displacement calculated for the Kalapana fault source in Table 2, the start of the 1975 Kalapana tsunami. The fault slip is limited in horizontal extent to reproduce only the region of largest deformation, especially the subsidence around Halape. Activity on the Kalapana fault probably extended further east, presumably to the epicenter of the main shock. However, this tsunami source does not account for subsidence in the region of Kalapana itself, in part because most of this deformation would have occurred on land and therefore not contributed to the tsunami. Far field deformations induced by the earthquake are depicted in the upper left and lower right hand corners. Fig. 5b provides the Geowave simulation results of maximum wave elevation above sea level for the Kalapana fault source, demonstrating a highly concentrated region of inundation, as would be expected for a near shore tsunami source of limited horizontal extent. Significant wave activity extends West to South Point due to edge wave propagation. There is also a far field beam of wave energy sent southeast by the parabolic shoreline around Halape, as well as the focusing effect of offshore thrust structures. As mentioned before, the Kalapana fault source is necessary to account for early wave activity observed in the region of Halape.

Fig. 5c describes the slump source in Table 3 with the same vertical wave amplitude scale in meters as Fig. 5a. This tsunami source captures the depression wave generated along the upper face of the slump as well as the elevation wave generated along the lower face of the slump. Its width is intended to cover the full extent of possible flank failure, with the maximum amplitudes concentrated along the axis of maximum deformation in an appropriate manner. The slump source was generated gradually overtime, which allows wave activity to propagate both east and west during tsunami generation, beyond the edges of slumping. This increases the source with relative to the slump width, and decreases the tsunami amplitude somewhat (Watts et al., 2002, 2003). Fig. 5d provides the Geowave simulation results for the slump source, with the same maximum wave elevation above sea level and the same wave amplitude scale in meters as Fig. 5b. The wave amplitude scale saturates at 2 m despite much larger tsunami amplitudes in order to discern far field wave activity. The slump source attacks the south shore of Hawaii to a much greater extent than other regions around the island. A powerful beam of wave energy is also sent southeast into the far field. It will soon emerge that the slump source describes much of the wave activity along the south shore of Hawaii, thereby providing an essential contribution to the 1975 Kalapana tsunami.

Fig. 5e shows the thrust fault source in Table 4, presumed to arise rapidly near the end of slumping. As mentioned before, the vertical coseismic displacement of this tsunami source would occur over and above the slump motion, which serve the role of a mechanical amplifier with regard to tsunami generation. At first glance, the thrust fault source may seen oddly out of place. However, key features (“Elevation” and “Depression”) of the thrust fault source in Fig. 2e correlate with regions of bathymetric elevation (“Thrust Structures”) and depression (“Western Ridge”) in Fig. 2b, respectively, providing strong support for both mechanism and location of

seismic activity. That is, what went up in 1975 corresponds to bathymetric highs, whereas what went down in 1975 corresponds to bathymetric lows. This is consistent with our earlier point that large total displacements. Kilauea deformation is once again predicted to induce vertical coseismic displacement reaching into the far field. Fig. 5f provides the Geowave simulation results for the thrust fault source. The thrust fault source attacks much of the shoreline of Hawaii, with the notable exception of the region around Halape. The thrust source appears to send significant wave energy around the sharp eastern and western corners of the southern shoreline of Hawaii, no doubt because it lacks the inherent directivity of the slump source and because it occurs further offshore. However it would be *incorrect* to conclude here that the slump source fails to propagate significant wave activity to other Hawaiian Islands, and that far field wave activity is the exclusive domain of the thrust fault source. It is *correct* to state that for the island of Hawaii, specifically, the thrust fault source is necessary to account for much of the wave activity along the eastern and western shores.

We provide a note of caution here on account of the *form* with which simulation results appear in Fig. 5. The maximum wave elevation above sea level is a useful measure of wave activity, and clearly differentiates three patterns of tsunami attack between the three tsunami sources, respectively. However, the maximum wave elevation is stripped of its temporal information, which means that there is no simple way to predict the same result for the combined tsunami sources, neither by the sun nor the mean nor the maximum. A linear superposition of three temporal records can just as easily cancel out individual maxima as it can superpose these maxima, and the only way to find the interference pattern is to run the simulation. Once again, this is a consequence of our *chosen representation* of the simulation results, and does not impact the actual superposition of wave activity, which will retain the same patterns of tsunami attack shown in Fig. 5. We run our stimulation of the 1975 Kalapana tsunami in order to superpose the three tsunami sources at appropriate times, and to evaluate subsequent wave interference patterns, which will be highly localized.

3.4. Simulation of the 1975 Kalapana tsunami

Our simulation of the 1975 Kalapana tsunami has many interesting features: it is a direct (as opposed to inverse) simulation of the observations, it covers both the near field and the far field simultaneously, it is derived from our synthesis of geological data, and it contains multiple tsunami sources. We remind the reader that the distinct patterns of wave activity demonstrated by Fig. 5 represent natural outcomes inherent to each tsunami source. Therefore, the apparently distinct roles played by each tsunami source were not anticipated. Despite such a welcome simplification, it is worth remembering that each tsunami source remains poorly constrained, and is defined by many input parameters.

We perform a numerical simulation of the 1975 Kalapana event by combining the three tsunami sources of appropriate times. The Kalapana fault source defines the start of the simulation. The slump source is introduced at $t=t_0\cong 131$ s as determined by TOPICS through an estimate of the duration of slump acceleration (Watts, 1998, 2000; Watts et al., 2002, 2003). The thrust fault source, arising from a low frequency seismic event of significant duration, requires us to choose a specific time with which to introduce the source, which is theoretically instantaneous according to elastic deformation theory. We know that there will be a delay on the order of 1 min between rupture of the Kalapana fault and significant rupture at the toe of the slump, on account of the finite propagation speed of shear waves from the headwall to the toe of the slump. The motion of the thrust complex itself will have some finite duration as the slump builds up compressive stress at its toe, further delaying development of the tsunami source. Therefore, we choose to introduce vertical coseismic displacement from the thrust fault source at 131 s, or at the same time as the slump source, as the only reasonable time to which we can point. We are effectively saying that the thrust complex finishes rupture and tsunami generation at around that same time that the slump achieves its fastest motion. The thrust fault could just as easily rupture several minutes later, after slump motion. The thrust fault could just as easily rupture several minutes later, after slump motion ceases, but such a delay would be somewhat arbitrary. We return to this timing issue in Section 4.

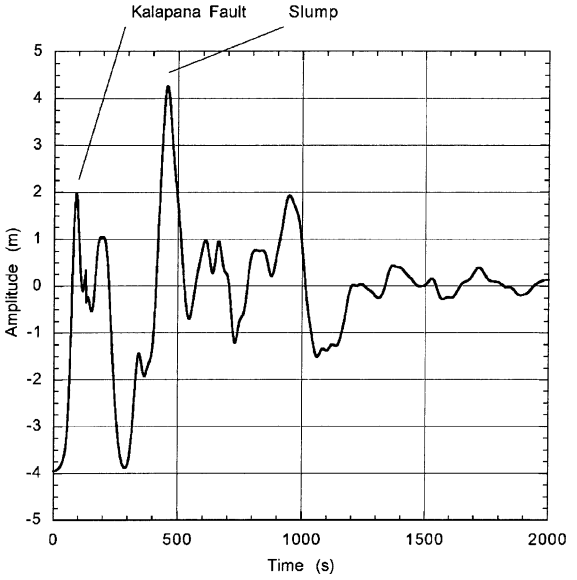

Fig. 6. Synthetic tide gauge record for Halape from the combined source simulation: note the presence of two discrete tsunami attacks separated by several minutes, as observed by eyewitnesses.

At Halape the simulation results presented in Fig. 6 compare favorably with the observations listed in Table 1. The free surface depression at the origin was not observed, because the coastal subsidence and vertical coseismic displacement are presumably identical at t=0 s. Our simulation does not make this distinction between reference frames, because the shoreline in our simulation is the *hypothetical* shoreline that would exist just *after* vertical coseismic displacement has finished. This is a different reference frame than the observations. Regardless of these definitions of shoreline, the depression wave is real relative to global sea level, which is not subject to such a change in local reference frame. Shortly after the main shock ceases, at around t=100 s, the shoreline is attacked by two elevation waves generated by the Kalapana fault. Our modelling results reproduce the eyewitness observations and support the existence of the Kalapana fault, because the early wave action requires a near shore fault, as opposed to an extensive region of offshore subsidence. A large withdrawal associated with the depression wave of the slump source is then followed by a second elevation wave generated foremost by the slump, according to the wave propagation results presented in Fig. 5. There may be some modest wave activity associated with the thrust fault after around t=500 s, although this is presumably masked by the slump source. By the end of the second tsunami attack, the tsunami hazard steadily decreases in tandem with the wave amplitudes and wave steepness. These results are a natural outcome of the three tsunami sources, as anticipated in Section 1.

Fig. 7 shows the progression of wave activity around Hawaii at six regular intervals of about 24 s. The snapshots are from shaded relief maps that indicated the orientation of the surface normal gradient along a northwest–southeast axis, a somewhat natural way to perceive surfaces, even though it tends to obscure actual elevations and depressions. Therefore, we described the wave activity in Fig. 7 frame by frame.

a. The slump and thrust fault tsunami sources have already been introduced, and small amplitude waves with short wavelengths appear on top of the evolving sources as the Boussinesq propagation model responds to the natural roughness of the bathymetry. Halape is still inundated from the initial tsunami attack, while the second elevation waves forms farther offshore.
b. The coastline west of Halape is undergoing withdrawal from a leading depression wave, as an elevation wave approaches from just offshore. The coastline east of Halape is experiencing tsunami attack from an elevation wave. At Halape itself, the ocean has withdrawn in anticipation of the slump generated elevation wave. Most of the small wavelength waves southeast of Kilauea are in a broad depression that is in the midst of a rebound.
c. In the west, the leading depression wave has already refracted around South Point while the subsequent elevation wave has just arrived. Likewise, the leading elevation wave has already rounded Cape Kumukahi, which is about to experience the subsequent depression wave. East of Halape, a sequence of edge waves propagates along the shoreline, while a broad elevation wave attacks the shoreline west of Halape.
d. In the west, the leading depression wave has begun propagating north along the Kona coast (Fig. 1), while the leading elevation wave is about to enter Hilo harbor in the east. The southern

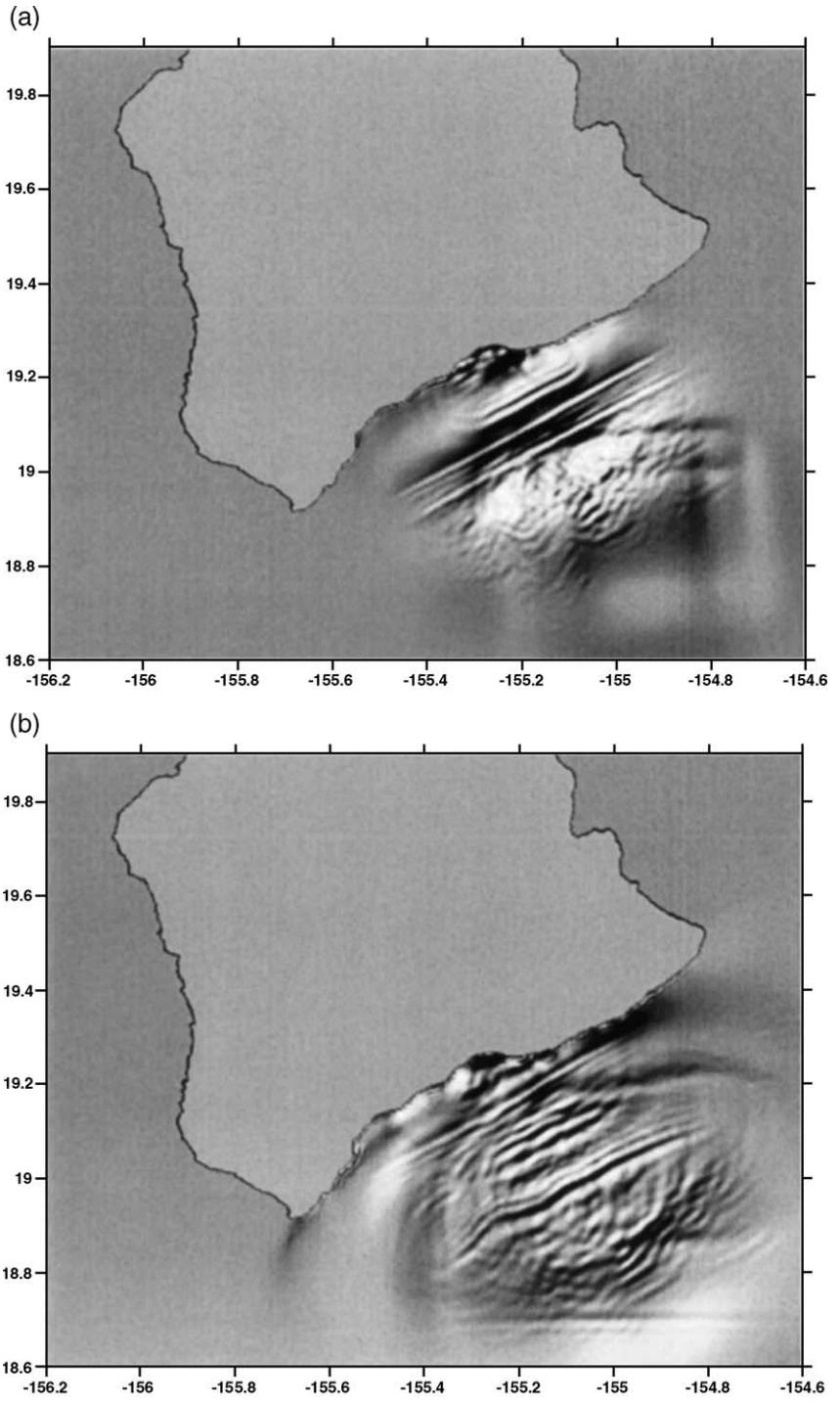

Fig. 7. Shaded relief maps of the combined source simulation showing snapshots of the free surface at (a) 204 s, (b) 407 s, (c) 611 s, (d) 815 s, (e) 1018 s, and (f) 1222 s. See the text for a description of wave action. The light source is in the northwest at a 45° angle of incidence from horizontal.

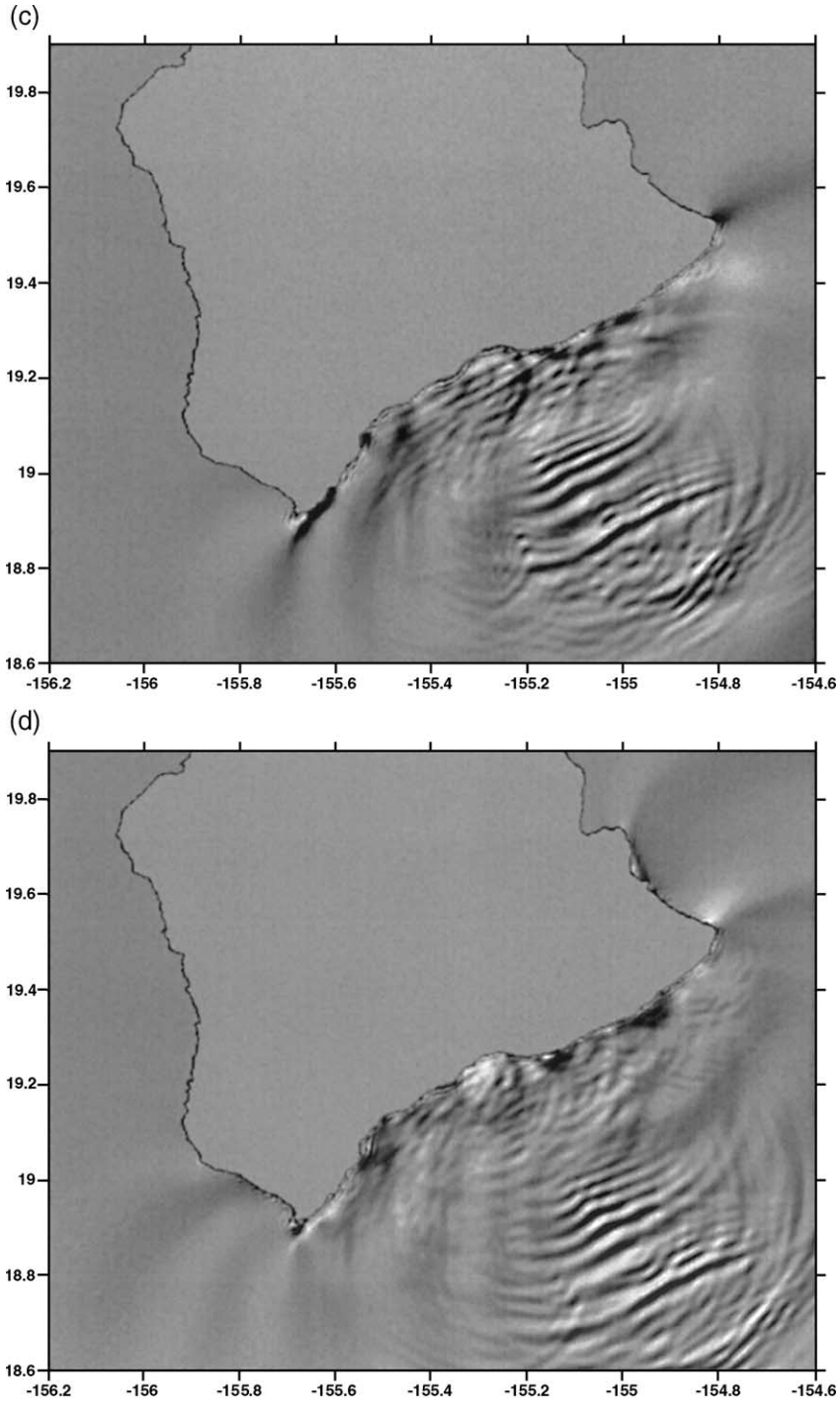

Fig. 7 (*continued*).

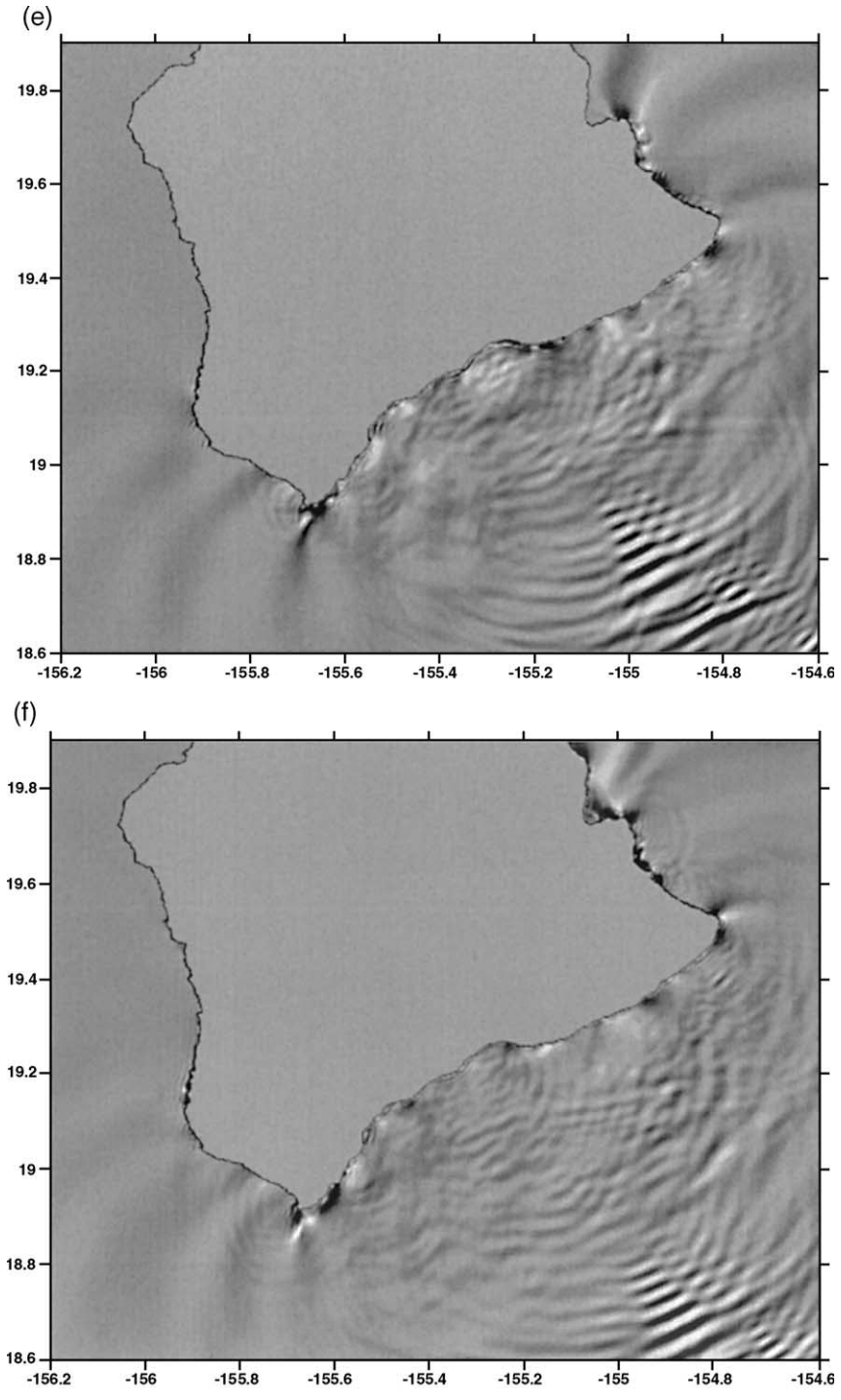

Fig. 7 (*continued*).

shoreline of Hawaii exhibits even more complex edge wave activity, while small wavelength waves radiate southeast, a consequence of various shoreline reflections and interactions.

e. In the west, an elevation wave has begun propagating north along the Kona coast. At Hilo, the leading wave has entered the harbor, while the subsequent depression wave is refracting towards the west as it rounds the point off Hilo. Constructive interference in the wave train headed southeast is producing a relatively focused beam of wave energy propagating into the far field.

f. In the west, the first elevation has propagated halfway up the Kona coast. Hilo has already been attacked by the leading elevation wave, while a depression wave enters the harbor. Just east of Hilo, an elevation wave is rounding the point in the form of a large amplitude edge wave. Along the south coast of Hawaii, edge waves continue dispersing and radiating energy into the far field, as wave activity diminishes in the tsunami generation region.

Figs. 8 and 9 depict the near field and far field maximum tsunami elevations above sea level, respectively. Fig. 8 is intended to be compared directly with the results in Fig. 5 by using the same wave amplitude scale (0–2 m). The reader will recall that the amplitude scale saturates 2 m in order to visualize offshore wave activity. As a first approximation, Fig. 8 appears to be a relatively simple combination of the dark regions made by the slump and thrust fault sources separately. Upon closer inspection however, the combined slump and thrust fault sources have increased wave activity along the east shore of Hawaii, and decreased wave activity along the west shore of Hawaii. These results may be simple consequences of constructive and destructive interference of the slump elevation wave with the thrust fault source, respectively. The near field simulation was run on a uniform 400 m grid. Fig. 9 uses a smaller wave amplitude scale (0–1 m) in order to visualize far field, wave activity among the Hawaiian Islands. In the far field, significant wave activity has been directed towards multiple shorelines because of bathymetric features. These include the eastern shore of Kohala on Hawaii, the eastern tip of Maui, Kahului bay on Maui, the southern shore of Lanai, and the southern shore of Oahu next to Penguin Bank (Fig. 9). A tsunami along the south shore of Hawaii can apparently present hazards to

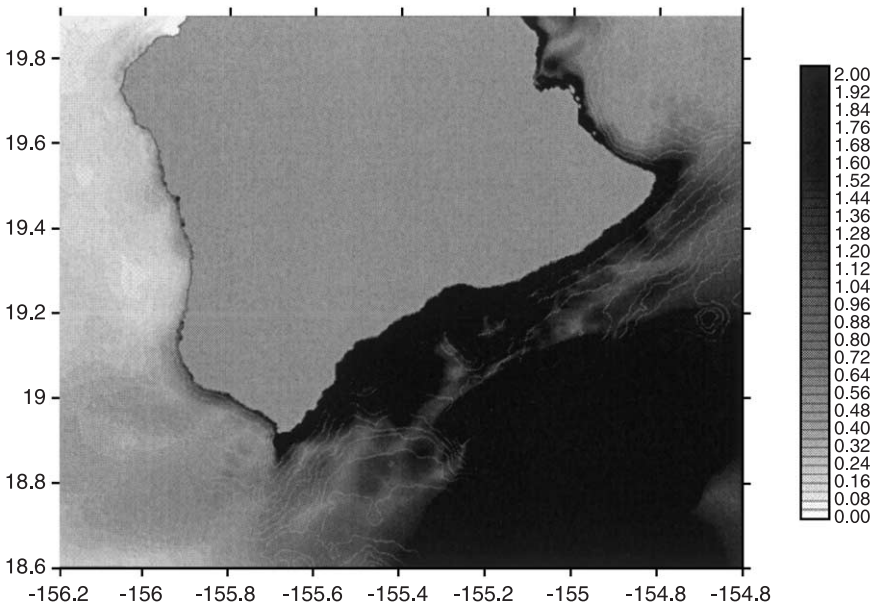

Fig. 8. Maximum tsunami elevation above sea level in meters for the combined source simulation carried out for the island of Hawaii.

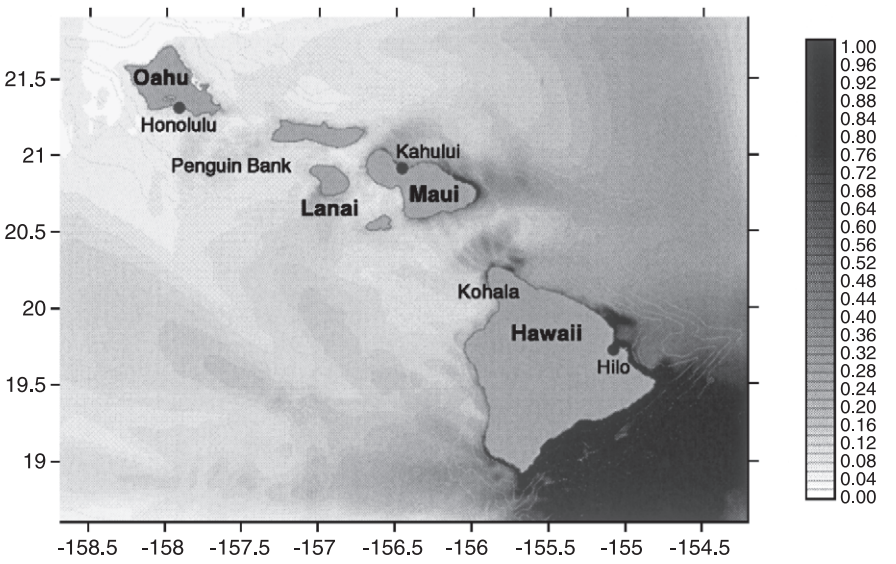

Fig. 9. Maximum tsunami elevation above sea level in meters for the combined source simulation carried out for some of the Hawaiian Island. Tide gauges are located at Hilo, Honolulu, and Kahului.

other Hawaiian Islands. The far field simulation was run on a uniform 1000 m grid.

Table 5 compares the observed and predicted maximum tsunami elevations above sea level at the Hawaii Island locations indicated in Fig. 1. The predicted values were taken from the same numerical simulation data shown in Fig. 8. When considered in its entirety, the agreement between observations and predictions is quite good. There are several ways to quantify this assertion. First, we calculated relative errors at each location by subtracting the predicted maximum elevation from the observed maximum elevation, and dividing by the observed maximum elevation. The mean relative error for all locations in Table 5 is only 3%, although there is a large scatter bounded by relative errors of less than ±95%. The standard deviation of relative errors for all locations in Table 5 is ±55%. Second, we curve fit a straight line going through the origin to observed *versus* predicted maximum elevation values. We obtained a slope of 0.97 with an r^2 value of 0.76. These results provide a reasonably strong correlation, given the geological uncertainty, and can be considered to enable maximum elevation predictions from the numerical simulation results.

As this section presents a direct numerical simulation of the 1975 Kalapana tsunami, we do not attempt to revise our tsunami sources in order to reduce the scatter in Table 5. We believe that the current geological data may not support making such revisions at this time, because the tsunamigenic structures are poorly constrained. In more precise engineering terms, there at least six slump input parameters in Table 3 (x_0, y_0, b, T, w, d) and at least two thrust fault input parameters in Table 4 (d, Δ) that could vary considerably. In addition, the timing thrust fault source remains uncertain, and mechanical connections between tsunami sources could be much more complicated than presented in Section 3.2. With so many important parameters in play, we would not expect to find a unique and meaningful numerical simulation capable of reproducing all observations. Instead, we would expect to find many ways to improve our results, with little or no geological guidance to choose one way over another.

3.5. Tide gauge records

Fig. 10 compares the observed and predicted tide gauge records at Hilo, Honolulu, and Kahului (Fig. 9). As in Fig. 7, we return to temporal wave activity of the 1975 Kalapana tsunami, which is a more challenging measure of a numerical simulation. The tide gauge records consist of a small-amplitude

Table 5
Maximum tsunami elevations above sea level

Location	Observed	Predicted	Relative error
	(m)	(m)	(%)
Honokahau (W)	2.1	0.66	−69
Kailua (W)	3.4	0.78	−77
Kahaluu (W)	1.8	0.59	−67
Keauhou (W)	2.4	0.96	−60
Napoopoo (W)	2.4	1.6	−33
Honaunau (W)	1.8	1.2	−33
Milolii (W)	<1.8	1.3	−28
South Point (W)	6.7	12	79
Kaalualu (S)	4.0	7.7	93
Honuapo (S)	6.1	9.8	61
Punaluu (S)	6.1	8.3	36
Kalue (S)	9.4	5.1	−46
Halape (S)	7.0	6.5	−7
Apua Point (S)	14.6	12	−18
Kamoamoa (S)	6.4	4.2	−34
Kalapana (S)	2.6	3.8	46
Pohoiki (S)	2.4	4.2	75
Cape Kumukahi (S)	3.4	4.3	26
Hilo (E)	3.0	3.0	0

The locations listed here are shown in Fig. 1 and occur counter-clockwise around Hawaii Island. The location is identified as being on the west (W), south (S), and east (E) coasts of Hawaii Island. Observations are taken from Tilling et al. (1976). Predicted values are identical to those depicted in Fig. 8.

oscillation followed by the arrival of a large-amplitude wave train, with longer arrival delays at a more distant tide gauge locations. In our simulation, we predicted wave train arrival several minutes early at all tide gauge locations, errors that are too large to be explained by any reasonable tsunami source off Halape or Kalapana. A consistent error of several minutes suggests that further delays in the thrust source are necessary. Random errors of several minutes may also be typical for tide gauge records (see Fryer et al., submitted for publication). We overcome these timing difficulties by aligning the first elevation waves of the observed and predicted wave trains. The first significant elevation wave at Hilo (Fig. 10a) is observed to last much longer than the predicted wave, which suggest that the tide gauge was behaving like a low pass filter. The tide gauge at Honolulu, Oahu (Fig. 10b) experiences many more waves than the other two tide gauges, a fact that we attribute to the more complex bathymetry traversed by these waves, including submerged volcano Loihi on Kilauea and shallow Penguin Bank just southeast of Oahu, and to the additional time available for wave dispersion.

When comparing the observed and predicted tide gauge records side by side on two separate plots, we found that the two wave trains appeared very similar in shape. However, when compared on the same plots, as in Fig. 10, the time scales are seen to differ by around 45% for all tide gauges. That is the simulation time should be strained by an additional 45% for most predicted peaks and troughs to line to with observed peaks and troughs. It is as if the predicted tide gauge records were following the observed pattern of rising and falling, but with wave periods are consistently too fast. These timing errors suggest that we reconsider fundamental issues with the tsunami sources, a process we begin in Section 4. A strained time scale may represent broader and/or slower deformations of Kilauea than we estimated for our tsunami sources.

A noteworthy result is that some of the wave activity observed prior to the arrival of the wave train *on all tide gauges* is predicted to be part of the 1975 Kalapana tsunami. This fact seems to have been overlooked or discounted by others (e.g., Tilling et al., 1976; Ma et al., 1999), who attribute time of arrival solely to the wave train. In our numerical simulation, wave activity begins around t=0 s with the occurrence of coseismic displacement from rupture of the Kalapana fault. Based on our representation of the Kalapana fault, we find the rough approximations of a 5.4 mm wave at Hilo, a −0.4 mm wave at Honolulu, and a −1.3 mm wave at Kahului. In a relative sense, larger coseismic displacements are associated with the thrust structure: 21 mm at Hilo, −1.7 mm at Honolulu, and −2.2 mm at Kahului. There is ample evidence of these waves on the actual tide gauge records, often with a similar wave activity pattern, and with significantly *larger* observed amplitudes than we predicted from the earthquake tsunami sources. This suggests that these waves exist and that our assumption of far field coseismic displacement is reasonable, even conservative. The observed amplitudes suggest that Kilauea deformation may have been *larger* than we calculate from our tsunami sources here. While our use of the earthquake tsunami sources in the far field is admittedly approximate, we note that the length scales, slope angles, and material interfaces involved in Kilauea deformation are similar to most traditional calculations of coseismic displacement made for

subduction zones. The Pacific Plate can be expected to react to Kilauea displacement during the 1975 Kalapana event over distances much greater than the size of the volcano. Fig. 10 therefore provides a *general* lesson for tsunami interpretation: the actual tsunami arrival time may be earlier than the obvious large-amplitude wave train.

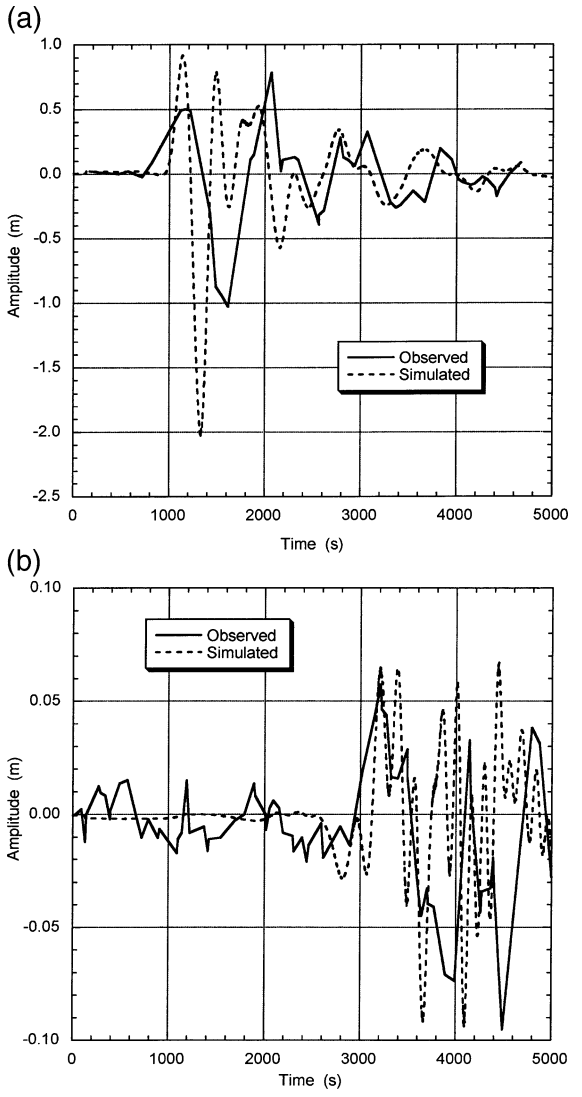

Fig. 10. Comparison of observed (solid) and combined source simulation (dashed) tide gauge records for (a) Hilo, Hawaii, (b) Honolulu, Oahu, (c) Kahului, Maui. Observed records were digitized from Ma et al. (1999) and have tidal oscillations removed.

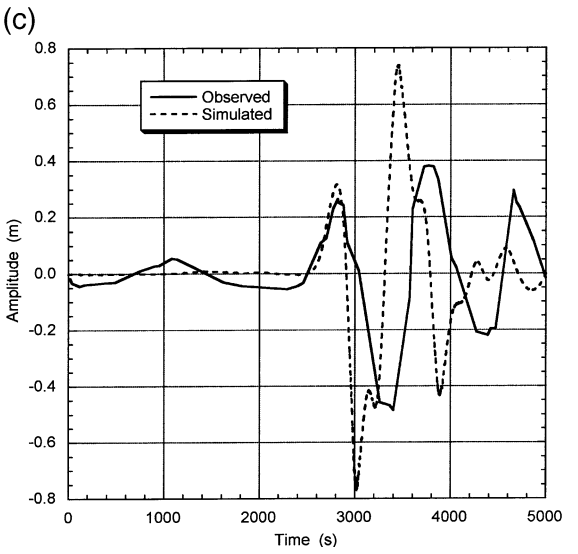

Fig. 10 (*continued*).

Table 6 compare the observed and predicted first elevation maxima and first depression minima of the large-amplitude wave trains shown in Fig. 10. The results vary from location to location. At Honolulu, the agreement between observed and predicted tsunami amplitudes is quite good. At Kahului, the predicted amplitudes are about 50% too large, possibly because this wave energy originates from the eastern side of Hawaii, which we noted earlier may have experienced constructive interference of the slump and thrust fault tsunami sources. We attribute the tsunami amplitude errors at Hilo to an inevitable error in the location of the synthetic tide gauge within Hilo harbor. We found strong node to node variation of maximum tsunami as an indication that wave activity was underresolved within Hilo harbor. We found strong node to node variation of maximum

Table 6
Comparison of observed and predicted tide gauge results

Selected tsunami amplitudes from wave train	Observed (m)	Predicted (m)
First elevation wave at Hilo, Hawaii	0.50	0.92
First depression wave at Hilo, Hawaii	−1.00	−2.00
First elevation wave at Honolulu, Oahu	0.057	0.065
First depression wave at Honolulu, Oahu	−0.074	−0.089
First elevation wave at Kahului, Maui	0.26	0.32
First depression wave at Kahului, Maui	−0.49	−0.77

Observations are taken from Ma et al. (1999).

tsunami amplitude above sea level on our 1000 m far field simulation grid, which we interpret as an indication that wave activity was underresolved within Hilo harbor for this grid. On shore at Hilo, we are still able to reproduce the maximum tsunami amplitude correctly in Table 5 with the near field grid, because of the better spatial resolution and because this value represents an aggregate of all wave activity around Hilo harbor. However, the tide gauge result remains very sensitive to the precise tide gauge location, which is only accurate to within ±500 m on our far field simulation grid.

4. Discussion on simulation results for the 1975 Kalapana tsunami

As we noted above, a deforming volcano can present complex geological structures in order to accommodate its deformation and geological evolution. The multiple ambiguities regarding seismic reconstructions of the 1975 Kalapana event (see Section 2) allow for many different geological structures. Just as it is difficult to commit to any single seismic event, it is also difficult to propose an isolated slump along the volcano flank. There had to be multiple tsunami sources. The same conclusion can be drawn from the tsunami observations, lending credence to multiple tsunami sources. We draw the line at three tsunami sources, because the geological data does not suggest any more similarly tsunamigenic structures to us, according to our current interpretation of the 1975 Kalapana event. Despite our confidence in the minimum number of tsunami sources, it is unreasonable to expect these three sources to be definitive. Both the quality of seismic records as well as the possibility of aseismic slip raises doubts as to the accuracy of the two earthquake sources. Our use of the approximate model TOPICS for the slump source is an appropriate indication of current geological uncertainty there. The issues we address in this section are fundamental: does our interpretation of geological structures withstand the lack of geological constraints on the tsunami sources? Is the coupling between geology and tsunami generation robust for this event? In both cases, the answer appears to be a qualified yes.

4.1. Near field observations

For the purposes of this subsection, we will consider simulation results for the island of Hawaii as constituting the near field, even though wave activity along the east and west coasts of Hawaii are better considered as being on the far field. The near field results present both successes and failures, as can be expected for such a complex event. The successes are perhaps best summarized by the predicted wave activity at Halape shown in Fig. 6 as well as the maximum tsunami elevations in Table 5. For any of these results, there is no a priori reason to have expected the three tsunami sources to capture observations of wave activity. We attribute these successes to careful consideration of multiple tsunami sources from volcano flank deformation. The coupling between geology and tsunami generation appears to be relatively robust for the 1975 Kalapana event.

Our failures become clear if one separates maximum tsunami elevations from Table 5 into distinct regions, such as the west coast of Hawaii, etc. Within each disparate region, it is not uncommon to find all maximum wave elevations to be 30–60% too small, or 30–60% too large, respectively. That is, while the near field results in Table 5 have tolerable relative errors that sum to around zero, the errors are hardly random. The regional pattern of tsunami activity is systematically biased, with too much tsunami energy along the east coast, and too little tsunami energy along the west coast. The radiation pattern of wave energy is intimately related to the free surface shape and location of a tsunami source, in addition to the intervening bathymetry. Consequently, we attribute the regional biases to inexact free surface shapes and locations of our tsunami sources, because the bathymetry is clearly correct.

One would be tempted to attribute errors to tsunami inundation as well, but we think that this is unlikely. We do not expect significant errors during tsunami inundation because the slopes off Hawaii are quite steep, *relative* to the free surface slopes of the incident waves, the shoreline therefore resembles to a vertical wall to a shoaling tsunami, regardless of grid size. Likewise, we do not expect significant tsunami propagation and inundation errors from our Boussinesq model *relative* to geological uncertainty. There-

fore, there is a tangible expression of geological uncertainty in our otherwise robust results, because the tsunami sources are clearly reasonable yet visibly biased. Some possible tsunami source changes include a different slump location or orientation, as well as more complex thrust structures, perhaps involving the oblique compressional structures of the Western Ridges (Morgan et al., 2003).

4.2. Far field observations

For the purposes of this subsection, we will consider stimulation results beyond the south coast of Hawaii as constituting the far field, a more appropriate definition for the 1975 Kalapana event. The far field tsunami is dominated by slump and thrust sources, which facilitates our analysis somewhat. At first, the far field results seem more ambiguous than the near field results discussed above. To begin with, the simulated amplitudes at the three tide gauges (Table 6) are uniformly too large. This is especially true at Hilo and Kahului, once again indicating too much tsunami energy headed east. An additional tsunami source projecting tsunami energy to the west may be needed, such as an additional thrust source for the Western Ridge, especially given the oblique nature of the current thrust source. Also, the ad hoc 45% straining of the simulated time scale is potentially disconcerting. However, the far field simulation results are not nearly as ambiguous as these observations suggest. They are in fact a source of optimism. And the strained time may in fact provide useful insight into our tsunami sources.

First of all, we compared our far field simulation results for the combined tsunami sources with simulations of the slump and thrust sources run in isolation. Simulations of the slump source alone, of the thrust fault source alone, and of the combined sources all produced very different synthetic tide gauge records at each location. Therefore, the synthetic tide gauge records in Fig. 10 have wave train shapes that are an integral consequence of the *combined* slump and thrust tsunami sources. This strongly suggests that neither source is spurious. Second, the wave train shape of a tide gauge record is perhaps the single most sensitive measure of any tsunami simulation. It is well known by tsunami scientists that the time of arrival and amplitude of the first wave on a tide gauge record can be simulated relatively easily under favorable conditions. It is equally well known that a Boussinesq propagation model may be needed to capture the finer aspects of time of arrival and subsequent wave train shape. Given that Fig. 10 suggests a 45% strained time at all tide gauge locations, especially at Honolulu, it follows that our proposed straining almost certainly has some basis in fact, and may even provide further insight into the 1975 Kalapana event.

We interpret the need for time straining as follows: the tsunami wavelength is about 45% too small, presumably from both slump and thrust sources, as they are mechanically interrelated. This may mean that the regions of deformation considered here are too small. Or, this may mean that the slump motion described by Table 3 is too fast. In colloquial terms, the slump and thrust sources are too concentrated in space and/or time. Some geological structures were either horizontally bigger or moved slower than specified. For example, the thrust source may have slipped gradually during 130 s (or more) and therefore allowed the tsunami wavelength to grow during tsunami generation. Or, uplift may have occurred over larger thrust structures (Fig. 2b), increasing the horizontal extent of the tsunami source shown in Fig. 5f. The impact of these tsunami source changes on our far field tsunami simulation would be to rescale the time base and redirect tsunami energy, both desirable effects that could improve simulation results. Regardless, we believe that the tsunamigenic structures identified in this work are in general correct, although more work is needed to constrain their spatial and temporal extent. Other tsunamigenic structures may have also played roles during the 1975 Kalapana event, but their identification and inclusion remains difficult at this time.

5. Long-term implications of the 1975 Kalapana event

As noted at the beginning of the paper, our objective is to produce a geologically realistic model for the 1975 Kalapana event that places it in the context of the overall deformation and geological evolution of the south flank of Kilauea. In the

previous sections, we have demonstrated that the tsunami can be explained in terms of movements on three structures: the proposed Kalapana normal fault, the slump structure, and the oblique thrust fault. In this section we consider how these structures may be mechanically related to each other. We then go on to consider how these structures may have developed as elements in the long-term geological evolution of Kilauea and the older Hawaiian volcanoes on which Kilauea has grown (Lipman et al., 2000, 2002). To begin this process, we examine the one new structural element that we have introduced in this paper, the proposed Kalapana fault.

5.1. Landward-dipping, north-facing normal faults at Kilauea

Normal fault scarps are among the most prominent topographic features of the south flank Kilauea, related to seaward-facing, south-dipping faults such as those of the Hilina–Holei fault system (Fig. 11a). These faults form scarps up to 500 m in height, with old lava flows (the Hilina formation basalts) exposed in places along the scarps, and with the rest draped by younger lavas. Although the fault scarps have been traced as far east as Kamoamoa area, around 8 km west of Kalapana, surface ruptures of the draping lavas are restricted to the western part of the Hilina–Holei fault system. Indeed, Cannon and Burgmann (2001) show that in a number of places it may be the case that the only surface ruptures on these faults during the past 400–750 yr are those associated with the 1975 Kalapana and 1868 Great Kau earthquakes. They estimate time-averaged vertical displacement rates of 2 mm/yr to 20 mm/yr over the past 750 yr for the entire Hilina–Holei fault system in sections between Puu Kapukapu and the Chain of Craters road (Fig. 2a). Further east, where no surface fault ruptures occurred in 1975, time-averaged displacement rates over the same period are presumably much lower. The disappearance of these faults to the east, well short of the eastern limit of coastal subsidence recorded in 1975 (Tilling et al., 1976; Lipman et al., 1985), supports the existence of our proposed Kalapana fault. The even more extensive subsidence associated with the 1868 earthquake (Brigham, 1909; Wyss, 1988) may have also been associated with movement on the Kalapana fault.

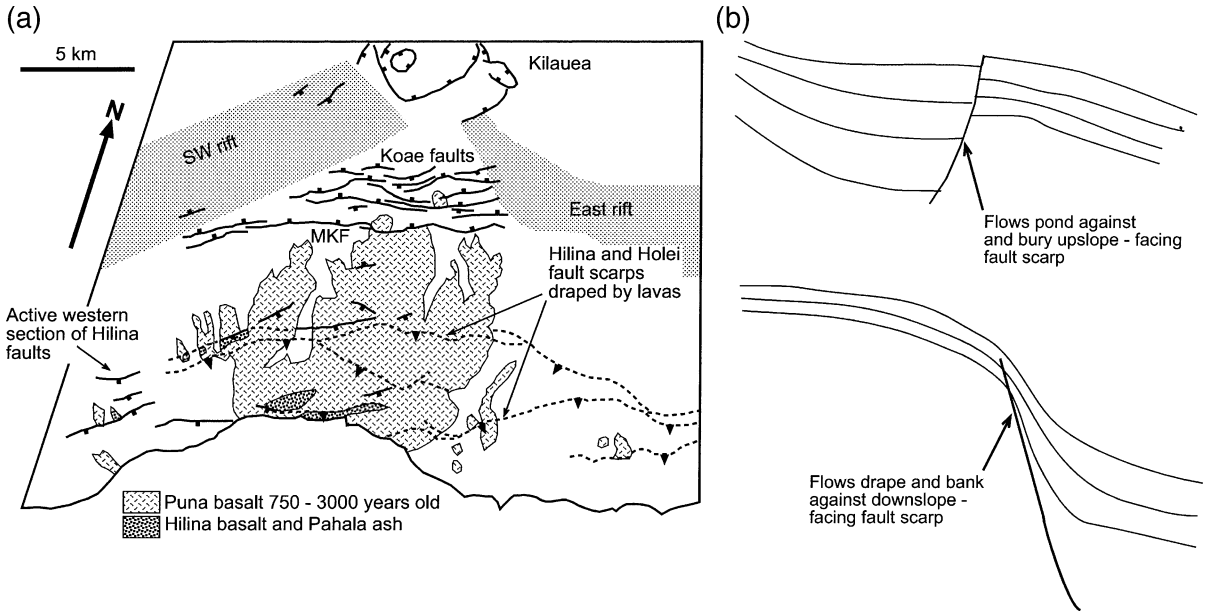

Fig. 11. (a) Map of Koae and Hilina fault systems south of Kilauea caldera, showing areas in which old lava flows and pyroclastic deposits of the Hilina Formation (Easton, 1978) and >~750 yr old lavas of the Puna Basalt Formation are still exposed (simplified from Wolfe and Morris, 1996). MKF indicates the position of the Kalanaokuaiki Fault. (b) The different relationships between surface-rupturing movement on the Koae and Hilina faults and fault-crossing lava flows.

Similar or higher displacement rates to those on the Hilina–Holei fault system can be inferred, again on the basis of offsets of several–hundred–year old lava flows, for the north-facing faults of the Koae fault system (Fig. 11a). The main fault in this system, the Kalanaokuaiki fault, displaces 600 to 1150 yr old flows by some 15 m vertically, implying a displacement rate around 20 mm/yr on this one fault alone. It has been proposed that Koae faults are a relatively recent features in the development of Kilauea, only some 1000 yr old (Duffield, 1975; Swanson et al., 1976). However, Parfitt and Peacock (2001) demonstrate from the dimensions of individual fault strands the Koae faults are a mature and long-lived fault system comparable in scale to Hilina–Holei fault system.

Despite their apparent maturity in structural terms, the Koae faults are a much less topographical obvious feature on Kilauea than the Hilina–Holei fault system (Fig. 2a). The reason for this is shown diagrammatically in Fig. 11b: lava flows descending from the Kilauea summit area tend to pond against north-facing fault escarpments, forming thick flows than can bury the escarpments, if flow accumulation rates exceed fault slip rates. Intermittent burial of Koae faults by lava flows also accounts for the apparent young age of the faults: we argue that only the upper lip and surface ruptures of the faults are young. In contrast, lavas will tend to flow over south-facing scarps as thin flows that do not obscure the accumulated topographic expression of the fault movements. Thus, the process of growth of Kilauea, by eruption of the lava flows from the summit region and from the rift zones, produces an inherent bias in the topographic preservation of seaward or south-facing faults, and against landward or north-facing faults. We therefore contend that the importance of north-facing normal faulting on Kilauea has been systematically underestimated in the past, including the proposed offshore Kalapana fault.

Fig. 11 also indicates another feature of the Koae faults. At present, these faults form distinct scarps up to 15 m high that block southward flow of lavas (most recently in 1974), leading to the continued exposure of older lavas in the area to the south of these scarps. However, the occurrence of several hundred to just over a thousand year old flows, south of the Koae fault system, points the period in which the Koae fault scarps were buried and lava flow to the south was unobstructed. Earlier periods in which accumulation of lavas in this area may have been blocked by the emergence of the surface fault scarps along the Koae faults are suggested by gaps in the sequences of lavas exposed in the Keana Bihopa and Puu Kapukapu fault escarpments (Fig. 2a) within the Hilina–Holei fault system (Easton, 1978, 1987). In addition, gaps in these sequences of lavas are associated with phreatomagmatic ash deposits implying that periods when the southward flow lava was blocked were also periods when Kilauea caldera was deep, and susceptible to large-volume phreatomagmatic eruptions (Easton, 1978, 1987; Dzurisin et al., 1995; McPhie et al., 1990).

Episodic activity may therefore be a feature of the Hilina–Holei fault system. As noted by Cannon and Burgmann (2001), the 1975 and 1868 earthquakes may account for most of the surface displacement on sections on these faults in the past several hundred years. Further east, the complete draping of the fault scarps by lavas in the age range 750 yr—present (Wolfe and Morris, 1996) suggests that this part of the Hilina–Holei system has not produced significant surface ruptures in this period. As noted above, in this same period the Koae faults have produced significant displacement. This suggests that the periods of activity on the Koae fault system and the Hilina–Holei fault system may alternate. If, so the Koae faults are not simply a conjugate set to the Hilina–Holei faults, as proposed by Parfitt and Peacock (2001), but also present alternating mechanical actions in the deformation of Kilauea volcano.

Since the proposed Kalapana fault has little surface expression and its subsurface structure remains uncertain, we cannot say at present whether it too an episodic movement history. However, its proximity to the fault systems upslope would suggest that further investigation of the Kalapana fault might reveal similar activity. Rapid local subsidence at the coastline suggests to us that the Kalapana fault is currently an active structure. This raises the possibility that the Kalapana fault ruptures in synchrony with the similar north-facing Koae faults. Alternatively, the Kalapana fault may rupture in synchrony with the Hilina–Holei fault system as two normal faults on either side of subsiding block as, in the 1975 Kalapana event. Either way, the Kalapana fault

is expected to play an integral role in Kilauea geological evolution.

5.2. The mechanics of the 1975 Kalapana event

The tsunami modeling results in Section 3 imply at least 3 tsunami sources for the 1975 Kalapana event. The sequence of three tsunami sources is inferred to have begun with slip on the Kalapana fault. This was followed by the movement of the slump and then finally by the oblique thrust event. The sequential triggering of these events, as well as their linkages to the initiating fault rupture itself, requires a mechanical or structural explanation in terms of the geological evolution of the south flank of Kilauea.

The structural geometry of the south flank of Kilauea is constrained by geological and geophysical surveys. The former have been compiled into the geological map of Hawaii (Wolfe and Morris, 1996). The recent reflection seismic profiles of Morgan et al. (2000,2003) and Hills et al. (2002) build upon the earlier studies of Hill and Zucca (1987) and Thurber (1987). The kinematics of deformation are similarly constrained by geodetic and seismic monitoring of the volcano (Lipman et al., 1985; Denlinger and Okubo, 1995; Owen et al., 2000; Cervelli et al., 2002). Fig. 12 summarizes the geometry of various structural elements of Kilauea in cross-section, through the region of the greatest deformation in 1975. Below the coastal graben structure, we suggest an accommodation zone where conjugate normal fault cross, and an immobile wedge at the volcano base, on either side of which deformation takes place. Deformation is seen to alternate horizontally between regions of compression and extension, starting with the compression of the magma body on the left and the ending with compression along the basal thrust on the right.

Table 7 summarizes our proposed kinematic characteristics of the different structural elements, both overall and during the 1974–1976 periods that includes the Kalapana earthquake. Critically, these include elements that deform episodically, and elements on which deformation is expected in large part to be continuous. The most important of the latter appears to be basal Thrust fault between the coast and the southeastern limit of the mid-slope bench, continuous or creeping movement on which accounts for the interseismic deformation monitored geodetically by Lipman et al. (1985) and Owen et al. (2000). Faults within the volcanic edifice above this section of the basal thrust also appear to deform aseismically (Cervelli et al., 2002). This behavior poses a problem for the mechanics of the 1975 earthquake, which

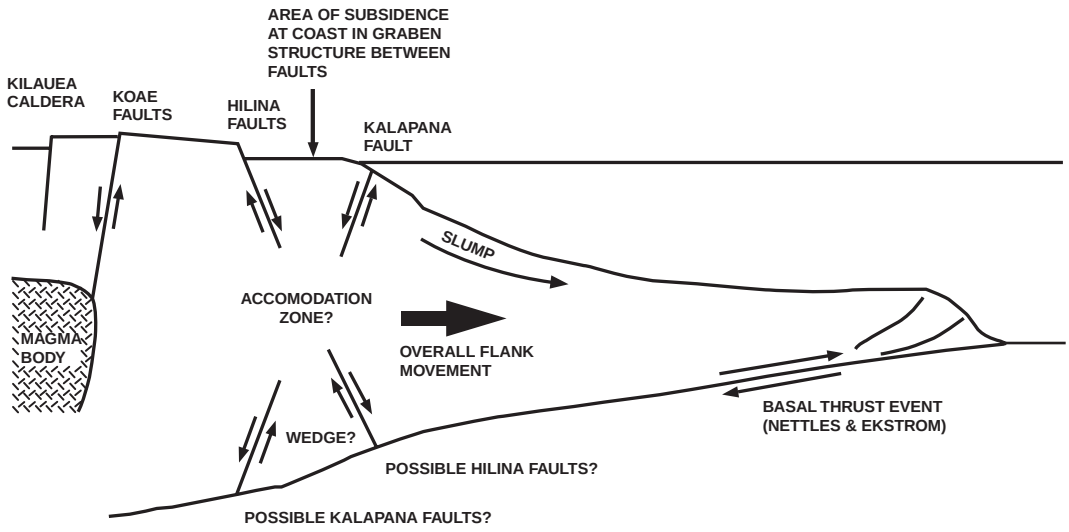

Fig. 12. Detailed cross-section describing the expected geometry and mechanical activity of the structural elements of Kilauea volcano that we infer to have been involved in the 1975 Kalapana event. Structural elements are consistent with Morgan et al. (2003). Black arrows indicate the preferred slip direction, whereas gray arrows indicate an implied slip direction.

Table 7
Kinematic behavior of structural elements of Kilauea

Structural element	General behaviour	Behaviour in 1974–1976
Koae faults	Largely locked	Slipped in 1975 earthquake
Basal thrust faults zone between summit rifts and coast	Slow deformation, compressing region between rifts and coast	Slipped in 1975 earthquake and continued aftershocks
Surface region of volcano between summit and coast	Generally in compression	Locally in extension 1974–1975 (Lipman et al., 1985). Abruptly extended in 1975 earthquake, shortened during aftershocks
Deep steeply dipping faults	Locked	Slipped at beginning of 1975 earthquake, triggering event (Bryan, 1992)
Kalapana fault	Locked	Normal fault movement at beginning of 1975 earthquake
Basal thrust fault between coast and mid-slope bench	Creeping: slow extension in coastal region	May have moved in 1975 earthquake; no aftershocks
Slump structure between Hilina faults and toe duplex	Creeping: slow slump movement, episodic more rapid movement	Abrupt slump movement by up to 90 m
Toe thrust duplex	Compression and uplift; not known if this is continuous or episodic (co-seismic)	Compressional thrusting forming last component of 1975 earthquake

involved rupture on faults both north and south of this continuously deforming section of the flank of the volcano. Creeping fault segments are believed to be barriers to fault rupture during earthquakes (Steinbrugge et al., 1960). How then did the different ruptures of the 1975 earthquake communicate with one another?

One possible explanation for the sequence of events may be that the 1975 earthquake ruptured through the creeping section, which then resumed its aseismic behavior and did not produce aftershocks. Another is that the transfer of the mass downslope in the slump produced additional loading of the toe thrust duplex identified by Hills et al. (2002) and so triggered the thrust earthquake downslope. The first explanation requires a coincidence between the duration of the slump movement and the length of time that the earthquake took to rupture through the creeping zone; the second has the advantage of explaining the sequence of displacements that we have inferred in order to produce the observed features of the tsunami. Slump loading of thrust structures is also reasonable explanation for the existence of three distinct tsunami sources. In general, flank deformation implies motion on multiple faults and failures planes.

5.3. Implications for the evolution and stability of the south flank of Kilauea

Studies of the south flank of Kilauea since 1975 show a highly complex volcano structure, with markedly different structural geometries and kinematic patterns of deformation at different depths and at different distances from the summit of the volcano. In particular, our analysis of slump motion suggests extremely low shear stress value between the ocean crust and the volcano flank. Catastrophic lateral collapse and giant landslides are known to have occurred at other Hawaiian volcanoes (Moore, 1964; Moore et al., 1989, 1994). Could a similar occur at Kilauea during the present epoch? The southern flank of Kilauea is flattening out, especially in its subaerial part, through displacement on landward-facing normal faults including the Koae and Kalapana faults. The same situation will have applied in earlier periods when these landward-facing faults were highly active (see Fig. 11). At other times, when the seaward-facing faults such as the Hilina–Holei faults were active, the southern flank of Kilauea may have been steepening overall and catastrophic slope failures, either of the entire flank or of section of the flank, may have been more likely. Although sections of the Hilina–Holei fault system at the extreme western end of the flank of Kilauea did rupture in 1975 (Tilling et al., 1976; Lipman et al., 1985), the overall volcano deformation includes extension and subsidence in the upper flank, as well as compression and uplift of the toe region, accompanied by slump movement. The net effect of repeated Kalapana events

may be to *stabilize* the volcano and make catastrophic failure of the flank *less* likely in the near term.

Acknowledgement

Partial funding was provided by the US National Science Foundation through grant CMS-0100223 made to STG and PW. Partial funding also provided by Applied Fluids Engineering, Inc. The authors are grateful for discussions with and/or reviews from Alberto Armigliato, Peter Cervelli, Dave Clague, Gerard Fryer, Juli Morgan, Gary McMurtry, Meredith Nettles, John Smith, and Dave Tappin. Mention of trade names if for the identification purposes only and does not constitute endorsement.

References

Ando, M., 1979. The Hawaii earthquake November 29, 1975: low dip angle faulting due to forceful injection of magma. J. Geophys. Res. 84 (B13), 7616–7626.

Brigham, W.T., 1909. The volcanoes of Kilauea and Mauna Loa on the island of Hawaii. Memories of the Bernice Pauahi Bishop Museum 2, 478–497.

Bryan, C.J., 1992. A possible triggering mechanism for large Hawaiian earthquakes derived from analysis of the June 1989 Kilauea south flank sequence. Bull. Seismol. Soc. Am. 82, 2368–2390.

Cannon, E.C., Burgmann, R., 2001. Prehistoric fault offsets of the Hilina fault system, south flank of Kilauea Volcano, Hawaii. J. Geophys. Res. 106 (B3), 4207–4219.

Cannon, E.C., Burgmann, R., Owen, S.E., 2001. Shallow normal faulting and block rotation associated with the 1975 Kalapana earthquake, Kilauea volcano Hawaii. Bull. Seismol. Assoc. Am. 91, 1553–1562.

Cervelli, P., Segall, P., Johnson, K., Lisowski, M., Miklius, A., 2002. Sudden aseismic fault slip on the south flank of Kilauea volcano. Nature 415, 1014–1018.

Chen, Q., Kirby, J.T., Dalrymple, R.A., Kennedy, A.B., Chawla, A., 2000. Boussinesq modelling of wave transformation, breaking and runup: II: 2D. J. Waterw. Port Coast. Ocean Eng., ASCE 126 (1), 48–56.

Crosson, R.S., Endo, E.T., 1982. Focal mechanism and locations of earthquakes in the vicinity of the 1975 Kalapana earthquake zone 1970–1979: implications for the tectonics of the south flank of Kilauea volcano, island of Hawaii. Tectonics 1, 495–542.

Denlinger, R., Okubo, P., 1995. Structured of the mobile south flank of the Kilauea volcano, Hawaii. J. Geophys. Res. 100 (B12), 24499–24507.

Duffield, W.A., 1975. Structured and origin of the Koae fault system, Kilauea volcano, Hawaii. U.S. Geol. Surv. Prof. Pap., vol. 856, 12 pp.

Dzurisin, D., Lockwood, J.P., Casadevall, T.J., Rubin, M., 1995. The Uwenkahuna ash member of the Puna basalt: product of violent phraetomagmatic eruptions at Kilauea volcano, Hawaii, between 2800 and 2100 ^{14}C years ago. J. Volcanol. Geotherm. Res. 66, 163–184.

Easton, R.M., 1978. The stratigraph and petrology of the Hilina Formation: the oldest exposed lavas of Kilauea volcano, Hawaii. Unpubl. MS thesis, University of Hawaii.

Easton, R.M., 1987. Statigraphy of Kilauea volcano. In: Decker, R.W., Wright, T.L., Stauffer, P.H. (Eds.), Volcanism in Hawaii, U.S. Geol. Surv. Prof. Pap., vol. 1350, pp. 243–260.

Eissler, H.K., Kanamori, H., 1987. A single force-model for the 1975 Kalapana, Hawaii, earthquake. J. Geophys. Res. 92, 4827–4836.

Fryer, G.J., Watts, P., Grilli, S.T., Kirby, J.T., 2005. Source constraints on the eastern Aleutian tsunami of 1946. J. Geophys. Res. (submitted for publication).

Furumoto, A.S., Kovach, R.L., 1979. The Kalapana earthquake of November 29, 1975: an intraplate earthquake and its relation to geothermal processes. Phys. Earth Planet. Inter. 18, 197–208.

Goldfinger, C., Kulm, L.D., Mcneil, L.C., Watts, P., 2000. Super-scale failure of the Southern Oregon Cascadia margin. J. Pure Appl. Geophys. 157, 1189–1226.

Got, J.-L., Frechet, J., Klein, F.W., 1994. Deep fault plane geometry inferred from multiplet relative relocation beneath the south flank of the Kilauea. J. Geophys. Res. 99, 15375–15386.

Grilli, S.T., Watts, P., 1999. Modeling of waves generated by a moving submerged body: applications to underwater landslides. Eng. Anal. Bound. Elem. 23 (8), 645–656.

Grilli, S.T., Watts, P., 2001. Modeling of tsunami generation by an underwater landslides in a 3D numerical wave tank. Proc. of the 11th Offshore and Polar Eng. Conf., Stavanger, Norway, vol. 3, pp. 132–139.

Grilli, S.T., Vogelmann, S., Watts, P., 2002. Development of a 3D numerical wave tank for modeling tsunami generation by underwater landslides. Eng. Anal. Bound. Elem. 26 (4), 301–313.

Guha, S.K., 2001. Induced earthquakes. Kluwer Academic Publisher, Dordrecht.

Hill, D.P., Zucca, J.J., 1987. Geophysical constraints on the structure of Kilauea and Mauna Loa volcanoes and some implications for seismo-magmatic processes. In: Decker, R.W., Wright, T.L., Stauffer, P.H. (Eds.), Volcanism in Hawaii, U.S. Geol. Surv. Prof. Pap., vol. 1350, pp. 903–917.

Hills, D.J., Morgan, J.K., Moore, G.F., Leslie, S.C., 2002. Structural variability along the submarine south flank of Kilauea volcano, Hawaii, from a multichannel seismic reflection survey. In: Takahashi, E., Lipman, P.W., Garcia, M.O., Naka, J., Aramaki, S. (Eds.), Hawaiian volcanoes: deep underwater perspectives. Geophys. Monogr. AGU, vol. 128, pp. 105–124.

Kawakatsu, H., 1989. Centroid single force inversion of seismic waves generated by landslides. J. Geophys. Res. 94 (B9), 12363–12374.

Kennedy, A.B., Chen, Q., Kirby, J.T., Dalrymple, R.A., 2000. Boussinesq modelling of wave transformation, breaking, and runup: I. 1D. J. Waterw. Port Coast. Ocean Eng., ASCE 126 (1), 39–47.

Lipman, P.W., Lockwood, J.P., Okamura, R.T., Swanson, D.A., Yamashita, K.M., 1985. Ground deformation associated with the 1975 magnitude 7.2 earthquake and resulting changes in activity of Kilauea volcano, Hawaii. U.S. Geol. Surv. Prof. Pap., vol. 1276, 45 pp.

Lipman, P.W., Sisson, T.W., Ui, T., Naka, J., 2000. In search of ancestral Kilauea volcano. Geology 28 (12), 1079–1082.

Lipman, P.W., Sisson, T.W., Ui, T., Naka, J., Smith, J.R., 2002. Ancestral submarine growth of Kilauea volcano and instability of its south flank. In: Takahashi, E., Lipman, P.W., Garcia, M.O., Naka, J., Aramaki, S. (Eds.), Hawaiian volcanoes: deep underwater perspectives, Geophys. Monogr. AGU, vol. 128, pp. 161–191.

Liu, P.L.-F., Yeh, H., Lin, P., Chang, K.-T., Cho, Y.-S., 1998. Generation and evolution of edge-wave packets. Phys. Fluids 10 (7), 1635–1657.

Ma, K.-F., Kanamori, H., Satake, K., 1999. Mechanism of the 1975 Kalapana, Hawaii, earthquake inferred from tsunami data. J. Geophys. Res. 104 (B6), 13153–13167.

McPhie, J., Walker, G.P.L., Christiansen, R.L., 1990. Phreatomagmatic and phreatic fall and surge deposits from explosions at Kilauea volcano, Hawaii, 1790 AD: Keanakakoi ash member. Bull. Volcanol. 52, 334–354.

Moore, J.G., 1964. Giant submarine landslides on the Hawaiian ridge. U.S. Geol. Surv. Prof. Pap. 501-D, 95–98.

Moore, J.G., Clague, D.A., Halcomb, R.T., Lipman, P.W., Normark, W.R., Torresan, M.E., 1989. Prodigious submarine landslides on the Hawaiian ridges. J. Geophys. Res. 94, 17465–17484.

Moore, J.G., Normark, W.R., Halcomb, R.T., 1994. Giant Hawaiian landslides. Annu. Rev. Plant Sci. 22, 119–144.

Morgan, J.K., Moore, G.F., Hills, D.J., Leslie, S.C., 2000. Overthrusting and sediment accretion along the Kilauea's mobile south flank, Hawaii: evidence for volcano spreading from marine seismic reflection data. Geology 28, 667–670.

Morgan, J.K., Moore, G.F., Clague, D.A., 2003. Slope failure and volcanic spreading along the submarine south flank of Kilauea volcano, Hawaii. J. Geophys. Res. 108 (B9), 2415.

Muller, J.R., Martel, S.J., 2000. Numerical models of translational landslides rupture surface growth. J. Pure Appl. Geophys. 157, 1009–1038.

Nettles, M., Ekstrom, G., 2004. Long-period source characterizations of the 1975 Kalapana, Hawaii earthquake. Bull. Seismol. Soc. Am. 94 (2), 422–429.

Okada, Y., 1985. Surface deformation due to shear and tensile faults in a half-space. Bull. Seismol. Soc. Am. 75 (4), 1135–1154.

Owen, S., Segall, P., Lisowski, M., Miklius, A., Denlinger, R., Sako, M., 2000. Rapid deformation of Kilauea volcano: global positioning system measurements between 1990 and 1996. J. Geophys. Res. 105 (B8), 18893–18998.

Parfitt, E.A., Peacock, D.C.P., 2001. Faulting in the south flank of Kilauea volcano, Hawaii. J. Volcanol. Geotherm. Res. 106, 265–284.

Peacock, D.C.P., Parfitt, E.A., 2002. Active relay ramps and normal fault propagation on Kilauea volcano, Hawaii. J. Struct. Geol. 24, 729–742.

Riley, C.M., Diehl, J.F., Kirschvink, J.L., Ripperdan, R.L., 1999. Palaeomagnetic constraints on fault motion in the Hilina fault system, south flank of Kilauea volcano, Hawaii. J. Volcanol. Geotherm. Res. 94, 233–249.

Smith, J.R., Malahoff, A., Shor, A.N., 1999. Submarine geology of the Hilina slump and morpho-structural evolution of Kilauea volcano, Hawaii. J. Volcanol. Geotherm. Res. 94, 59–88.

Stein, R.S., 1999. The role of stress transfer in earthquake occurrence. Nature 402, 605–609.

Steinbrugge, K.V., Zacher, E.G., Tocher, D., Whitten, C.A., Claire, C.N., 1960. Creep on the San Andreas fault. Bull. Seismol. Soc. Am. 50, 389–415.

Swanson, D.A., Duffield, W.A., Fiske, R.S., 1976. Displacement of the south flank of Kilauea volcano: the result of forceful intrusion of magma into the rift zones. U.S. Geol. Surv. Prof. Pap., vol. 963, 39 pp.

Tappin, D.R., Shipboard Scientists, 1999 (July 27). Offshore surveys identify sediment slump as likely cause of devastating Papua New Guinea tsunami 1998. Eos 80 (30), 329.

Tappin, D.R., Watts, P., McMurtry, G.M., Lafoy, Y., Matsumoto, T., 2001. The Sissano, Papua New Guinea tsunami of July 1998—offshore evidence on the source mechanism. Mar. Geol. 175, 1–23.

Tappin, D.R., Watts, P., McMurtry, G.M., Lafoy, Y., Matsumoto, T., 2002. Prediction of slump generated tsunamis: the July 17th 1998 Papua New Guinea event. Sci. Tsunami Hazards 20 (4), 222–238.

Tappin, D.R., Watts, P., Matsumoto, T., 2003. Architecture and failure mechanism of the offshore slump responsible for the 1998 Papua New Guinea tsunami.. In: Locat, J., Mienert, J. (Eds.), Submarine mass movements and their consequences. Kluwer Academic Publishers, Dordrecht, pp. 383–389.

Thomson, R.E., Rabinovich, A.B., Kulikov, E.A., Fine, I.V., Bornhold, B.D., 2001. On numerical stimulation of the landslide-generated tsunami of November 3, 1994 in Skagway Harbor, Alaska. In: Hebenstreit, G.T. (Ed.), Tsunami research at the end of a critical decade. Kluwer Academic Publishers, pp. 243–282.

Thurber, C.H., 1987. Seismic structure and tectonics of Kilauea volcano. In: Decker, R.W., Wright, T.L., Stauffer, P.H. (Eds.), Volcanism in Hawaii, U.S. Geol. Surv. Prof. Pap., vol. 1350, pp. 919–934.

Thurber, C.H., Gripp, A.E., 1988. Flexure and seismicity beneath the south flank of Kilauea Volcano and tectonic implications. J. Geophys. Res. 93 (B5), 4271–4278.

Tilling, R.I., Koyanagi, R.Y., Lipman, P.W., Lockwood, J.P., Moore, J.G., Swanson, D.W., 1976. Earthquake and related catastrophic events island of Hawaii, November 29, 1975: a preliminary report. U.S. Geol. Surv. Circ., vol. 740, 33 pp.

Walder, J.S., Watts, P., 2003. Evaluating tsunami hazards from debris flows. In: Locat, J., Mienert, J. (Eds.), Submarine mass movements and their consequences. Kluwer Academic Publishers, Dordrecht, pp. 155–162.

Watts, P., 1998. Wavemaker curves of tsunamis generated by underwater landslides. J. Waterw. Port Coast. Ocean Eng., ASCE 124 (3), 127–137.

Watts, P., 2000. Tsunami features of solid block underwater landslides. J. Waterw. Port Coast. Ocean Eng., ASCE 126 (3), 144–152.

Watts, P., 2001. Some opportunities of the landslide tsunami hypothesis. Sci. Tsunami Hazards 19 (3), 126–149.

Watts, P., 2004. Probabilistic predictions of landslide tsunamis off Southern California. Mar. Geol. 203, 281–301.

Watts, P., Grilli, S.T., 2003. Underwater landslide shape, motion, deformation, and tsunami generation. Proc. of the 13th Offshore and Polar Engrg. Conf., ISOPE03, Honolulu, Hawaii, vol. 3, pp. 364–371.

Watts, P., Borrero, J.C., Tappin, D.R., Bardet, J.-P., Grilli, S.T., Synolakis, C.E., 2002. Novel simulation technique employed on the 1998 Papua New Guinea tsunami. Presented at the 1999 IUGG General Assembly in Birmingham, UK, and published by the first author at www.appliedfluids.com/resume.html.

Watts, P., Grilli, S.T., Kirby, J.T., Fryer, G.J., Tappin, D.R., 2003. Landslide tsunami case studies using a Boussinesq model and a fully nonlinear tsunami generation model. Nat. Hazards Earth Syst. Sci. EGU 3 (5), 391–402.

Waythomas, C.F., Watts, P., 2003. Numerical simulation of tsunami generation by pryoclastic flow at Aniakchak volcano, Alaska. Geophys. Res. Lett. 30 (14), 1751–1755.

Wei, G., Kirby, J.T., 1995. Time-dependent numeric code for extended Boussinesq equations. J. Waterw. Port Coast. Ocean Eng., ASCE 121 (5), 251–261.

Wei, G., Kirby, J.T., Grilli, S.T., Subramanya, R., 1995. A fully nonlinear Boussinesq model for free surface waves: Part 1. Highly nonlinear unsteady waves. J. Fluid Mech. 294, 71–92.

Wells, D.L., Coppersmith, K.J., 1994. New empirical relationships among magnitude, rupture length, rupture width, rupture area, and surface displacement. Bull. Seismol. Soc. Am. 84, 974–1002.

Wolfe, E.W., Morris, J., 1996. Geologic map of the Island of Hawaii. United States Geol. Surv. Misc. Invest. Ser. Map I-2524-A, .

Wyss, M., 1988. A proposed source model for the Great Kau, Hawaii, earthquake of 1868. Bull. Seismol. Soc. Am. 78, 1450–1462.

Yin, A., Kelly, T.K., 2000. An elastic wedge model for the development of coeval normal and thrust faulting in the Mauna Loa–Kilauea rift system in Hawaii. J. Geophys. Res. 105 (B11), 25909–25925.